Chinese Journal of Chemical Engineering 60 (2023) 212–227

Contents lists available at ScienceDirect

Chinese Journal of Chemical Engineering

journal homepage: www.elsevier.com/locate/CJChE

Full Length Article

Enhanced adsorption of target branched compounds including antibiotic norfloxacin frameworks on mild steel surface for efficient protection: An experimental and molecular modelling study

Lingli Chen [1], Yueting Shi [1], Sijun Xu [1], Junle Xiong [2], Fang Gao [1,*], Shengtao Zhang [1,*], Hongru Li [1,*]

[1] College of Chemistry and Chemical Engineering, Chongqing University, Chongqing 400044, China
[2] Chongqing Kunding Environmental Protection Technology, Co., Ltd, Chongqing 400044, China

ARTICLE INFO

Article history:
Received 27 August 2022
Received in revised form 16 January 2023
Accepted 16 January 2023
Available online 16 February 2023

Keywords:
Branched compounds
Norfloxacin part
Adsorption
Anticorrosion
Mild steel

ABSTRACT

In this study, an approach was proposed to employ new target branched compounds (TBCs) including multiple antibiotic norfloxacin frameworks for intensified adsorption films to achieve super protection of mild steel in HCl medium. Thus, the TBCs containing bis/tri norfloxacin skeletons were synthesized by multi-step preparation route. In addition, the reference linear compound (RLC) including a single norfloxacin part was also synthesized. The chemical structures of these compounds were confirmed by various means. It was demonstrated that the TBCs could form the tough adsorption films on the surface of mild steel, which could be processed mainly through chemisorption effect. The electrochemical analysis suggested that the TBCs displayed superior corrosion inhibition performance for low carbon steel in 1.0 mol·L^{-1} HCl solution over the RLC (RLC, 87.80%; TBC1, 97.63%; TBC2, 98.35%), which was further understood by the molecular modelling. The isotherm adsorption plots were employed to analyze the spontaneous adsorption process of the TBCs on low carbon steel surface, and a prominent chemisorption could be inferred by the standard Gibbs free energy changes of the adsorption.

1. Introduction

Organic branched compounds, which are belongs to dendritic structural molecules, are composed of cores and branched skeletons. This means that based on molecular preconstruction, different branch parts can be connection with cores by chemical bonding to build a single branched molecule. It is noted that such a branched compound may be an "amplifier" if multiple functional groups are included for special purposes. Hence [1], branched compounds are found in a variety of fields such as optical, optielectronic and biomedical fields.

With the development of chemical industry, mild steel is inseparable from processing of products, since it has fine thermal conductivity, electrical conductivity and ductility. Hence, mild steel is widely applied in machinery, buildings, vehicles, aeronautics and astronautics, instruments, agriculture, military and the other fields [2]. Mild steel easily loses electrons during oxidation, forming positively charged Fe ions, which thus react with O_2, CO_2 and H_2O in the air to yield various metallic compounds such as hydroxide, carbonate, bicarbonate, *etc.* Therefore, severe rust is often formed on mild steel surface in the air, which may restrain its broad application prospects [3]. Hence, inorganic acid pickling is normally required to remove rust on mild steel. On the other hand, acid cleaning can lead to serious corrosion on mild steel surface, which may bring threatens to steel-based applications. Thus, it is necessary to achieve sufficient protection of mild steel in acid solution.

At the current, a number of ways are employed to prevent mild steel from corrosion in acid medium, such as inert metal coating and anodizing *etc.* [4–7]. In the recent decades, organic corrosion inhibitor method has been receiving intensive interests because of individual advantages of simple operation, convenient processing and low-costs. Normally, organic corrosion inhibitor molecules contain lone pair electrons or delocalized π electrons in polar functional groups, heterocycles, aromatic rings and unsaturated covalent bonds [8], which thus can chelate with Fe atoms bearing *d*-empty orbitals. Hence, these compounds may display chemical interactions with mild steel, and adsorption films are formed on metal surface, which can prevent the contact of attacking species

* Corresponding authors at: College of Chemistry and Chemical Engineering, Chongqing University, Chongqing 400044, China.
E-mail addresses: fgao@cqu.edu.cn (F. Gao), stzhang@cqu.edu.cn (S. Zhang), hrli@cqu.edu.cn (H. Li).

https://doi.org/10.1016/j.cjche.2023.01.015
1004-9541/

with mild steel surface, and thus the anticorrosion effect may be realized in acid medium. Green chemical engineering requires people to develop eco-friendly organic molecules as remarkably efficient corrosion inhibitors for mild steel, which means the achievement of super protection of metal at low concentrations of organic inhibitors. However, it is difficult to seek such friendly and effective organic corrosion inhibitors.

Therefore, one of main concerns in this study attempts to propose a method to reach the above purpose. For this aim, this work proposes to employed norfloxacin frameworks based branched compounds as the target inhibitors through molecular prebuilding. It is noted that norfloxacin is a common clinical medicine and non-toxicity to our humans and animals [9]. In particular, norfloxacin contains N-heterocyclic rings and π bonds and the other heteroatoms. Hence, the target branched compounds (TBCs) including double and triple norfloxacin frameworks may be strongly adsorbed to mild steel surface through chemical adsorption, thus hindering inorganic acid attacking metal surface. For comparisons, the reference linear compound (RLC) bearing a single norfloxacin skeleton was also studied.

2. Experimental

2.1. Materials and characterization

The target branched compounds (TBCs 1, 2) and the reference linear compound (RLC) were prepared in our own laboratory based on Fig. 1. The intermediates (I1, I2, I3) were also prepared followed by Fig. 1. The starting materials for synthesis of the studied compounds, such as norfloxacin (98%), 1,3,5-*tris*(bromomethyl)benzene (97%), α,α'-dibromo-*p*-xylene (98%) and benzyl bromide (98%) were purchased from the Sigma-Aldrich Chemical Corporation. The other chemical reagents including methanol, acetonitrile, dichloromethane, sodium hydroxide (NaOH), potassium carbonate (K_2CO_3), trifluoroacetic acid (TFA) and anhydrous sodium sulfate were obtained from the Acros Chemical Corporation.

The chemical structures of the intermediates and final compounds were characterized by ^{1}H NMR (600 MHz), ^{13}C NMR (125 MHz) and ^{19}F NMR (400 MHz) 1D spectra at room temperature (298 K) with a nuclear magnetic resonance instrument (Bruker Corporation). The NMR peak of tetramethyl silane (TMS) was used as a reference point to identify the chemical shifts of NMR peaks of the samples. The FT-IR spectroscopy of the samples was determined by a Nicolet iS50 Fourier transform infrared spectrometer (Thermo Scientific Apparatus Corporation). The COSY spectra of the target samples (2D ^{1}H NMR spectra, 400 MHz) were performed with nuclear magnetic resonance instrument (Avance Neo 400). The element analysis of the studied compounds was surveyed with a CE440 elemental analysis meter from the Exeter Analytical Inc. The mass spectrometry of the target molecules was measured by an ESI (Electro-Spray Ionization)-MS technique with a Waters Acquity SQD. The detail synthesis and characterization were provided in Supplementary Material.

2.2. Surface characterization of mild steel

The metal samples were machined from mild steel ASTM A283C (American Society for Testing and Materials, 10 cm × 10 cm × 1 cm) containing 0.23% (mass) C, 0.17% (mass) Si, 0.40% (mass) Mn, <0.05% (mass) S, <0.045% (mass) P and the rest was Fe. The polished steel surface was carried out with 400, 800, 1200, 2000, 3000, 5000 grits SiC waterproof sandpaper, respectively. Then, the steel samples were further rapidly washed with deionized water and absolute ethanol and dried under vacuum. Then, immediately immersed

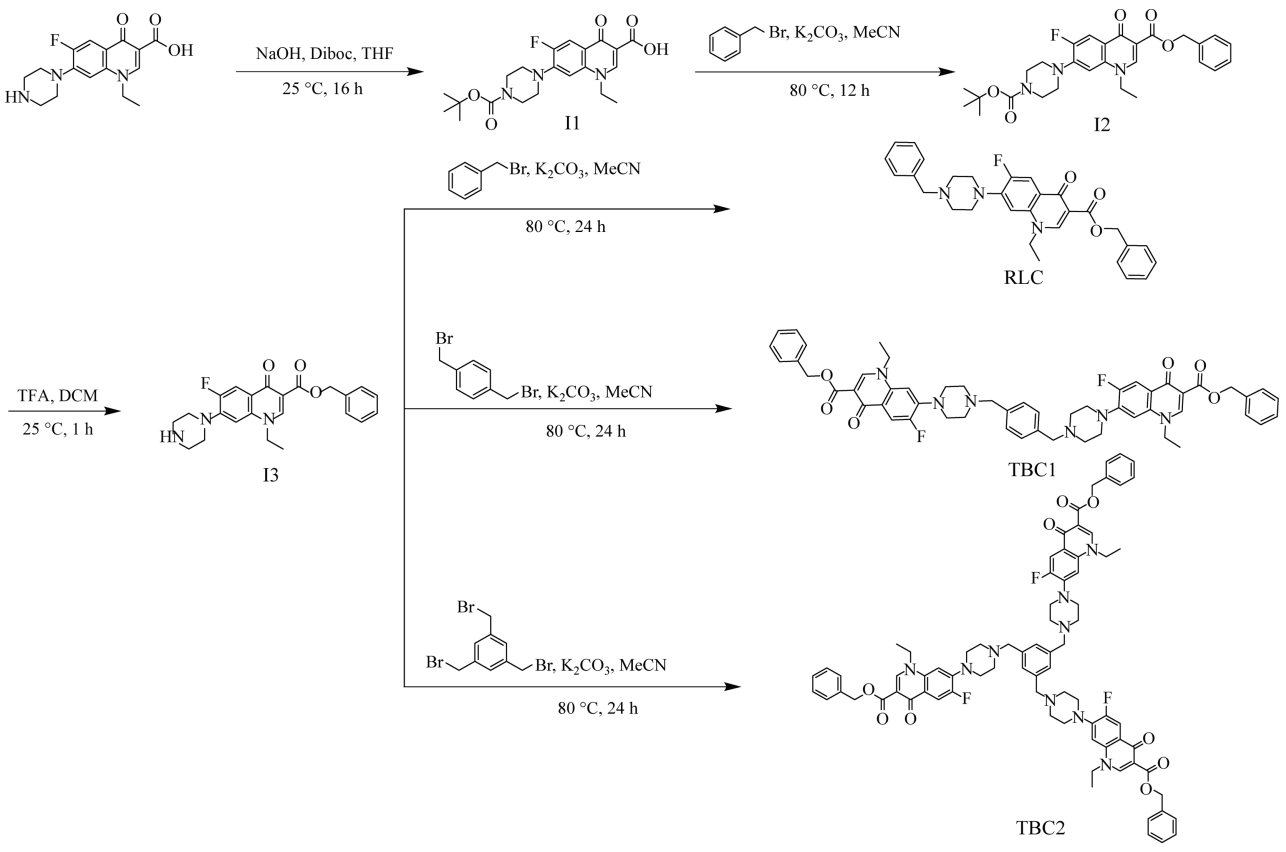

Fig. 1. Chemical structures and synthesis routes of the studied compounds.

the polished mild steel in a mixed DMSO/HCl solution (0.01 mol·L^{-1}) (volume ratio, 80/20) containing the studied compounds (TBCs and RLC) for 8 h to reach the self-adsorption equilibrium.

The adsorption behaviors of the studied compounds on mild steel surface were further confirmed and studied by scanning transmission electron microscopy (SEM), atomic force microscopy (AFM), X-ray photoelectron spectroscopy (XPS) and X-ray diffraction (XRD). The determination was performed by a PHI 5700 spectrometer equipped with an Al K_α X-ray source (1486.6 eV) corrected for the C 1s aliphatic carbon contamination peak at 284.8 eV [10]. The surface roughness of mild steel uncovered and covered by the studied compounds was investigated by AFM (MFP-3D-BIO, Asylum Research, America), respectively. The surface morphologies of blank steel and steel samples adsorbed by the investigated molecules were surveyed by SEM (Jeol-JSM-3.5 CF, Japan) at an accelerating voltage of 5.0 kV. The element energy dispersive spectroscopy (EDS) of the metal surface covered by the RLC and TBCs was carried out by an EDS system (EDAX EDS Element, America). All the measurements were conducted at the room temperature.

2.3. Electrochemistry analysis

All the electrochemical experiments were performed with a CHI660C electrochemistry working station (Shanghai Chenhua). The measurements were based on a conventional three-electrode system. The processed mild steel was used as the working electrode, saturated calomel electrode (SCE) was employed as the reference electrode, and a 2.0 cm × 2.0 cm platinum electrode was utilized as the counter electrode.

All potentials obtained in electrochemical tests are based on open circuit potentials (OCPs) measurements. Therefore, an open circuit potential test for 1800 s was required to ensure that the surface of the mild steel electrodes reached a stable state, thereby obtaining the stable voltage.

Once a stable open circuit voltage was obtained, the electrochemical impedance spectroscopy (EIS) experiments could be further conducted. The initial voltage was the measured stable E_{OCP} value, the sweep frequency ranged from a high frequency 100 kHz to a low frequency 0.01 Hz, and the amplitude of the AC interference signal was 5.0 mV. Finally, the corresponding equivalent circuit diagram was employed to perform simulation analysis through a ZSimp Win3.10 software, and the corresponding electrochemical impedance parameters were gained. The corrosion inhibition efficiency based on the electrochemical impedance was computed by Eq. (1) [11]:

$$\eta_E = \frac{R_{ct} - R_{ct,0}}{R_{ct}} \times 100\% \quad (1)$$

wherein $R_{ct,0}$ and R_{ct} represented the charge transfer resistance of the electrodes unadsorbed and adsorbed by the studied compounds, respectively.

The potentiodynamic polarization curve (Tafel) was further tested, the polarization potential range was E_{OCP} ± 0.25 V, and the polarization scanning rate was 1.0 mV·s^{-1}. The corrosion inhibition efficiency based on the potentiodynamic polarization curve was computed by Eq. (2) [12]:

$$\eta_j = \frac{I_{corr,0} - I_{corr}}{I_{corr,0}} \times 100\% \quad (2)$$

wherein $I_{corr,0}$ and I_{corr} showed the corrosion current density of the electrodes unadsorbed and adsorbed by the studied compounds, respectively.

In order to gain good reproducible data, three electrochemical experiments were performed under the same conditions as above.

2.4. Molecular modelling

The molecular geometry optimization of the target molecules TBC1 and TBC2 (the original forms) was conducted with a Gaussian 09 software on the basis of the density functional theory (DFT) [13]. The geometrically optimized molecules were acquired by using the B3LYP method with a 6-311++G (d, p) basis set [14]. The mixed solvents of DMSO/0.01 mol·L^{-1} HCl solution (80/20, volume ratio) were used as the medium in the optimization computation. The quantum chemical indices, such as the Mulliken charges, the highest occupied molecular orbitals energies (E_{HOMO}), the lowest unoccupied molecular orbitals energies (E_{LUMO}) and the energy gaps ($\Delta E = E_{LUMO} - E_{HOMO}$), the electronegativity (χ), the hardness (η), softness (σ) and charge transfer fraction (ΔN), dipole moment (μ) were acquired and analyzed [15].

Furthermore, the protonation forms of the studied molecules were also optimized. The protonated forms used in the optimization computation were analyzed to have the similar pK_a values to that of the medium (with a prediction software of ACD/Percepta v2020.1.0 based on classic algorithm). Thus, it is considered that these predicted protonated forms can be the most possible structures among the protonation forms. The molecular geometry optimization was performed as the above-described for the original forms.

3. Results and Discussion

3.1. Synthesis and characterization

The TBCs were successfully synthesized and the chemical structures were fully verified. For example, the single ^{1}H NMR peak of H (i) (δ_H, 1.563) (1D^{1}H NMR) indicates that the Boc group was introduced to yield the I1 (Boc-norfloxacin). The peaks of H (c, d) (δ_H 7.334 and 7.322) suggest that a benzyl bromide fully reacted with the I1 to give the I2. The lost NMR peak of the Boc group means that a full deprotection of Boc was finished and the I3 was yielded (please see the molecular characterization, SI). It is shown that the Boc group could be easily introduced and removed during the synthesis. In addition, the peaks of H (d, f) (δ_H 7.343 and 5.378) show that a benzyl bromide might well react with the I3 to give the final compounds.

The NMR peaks of H (d, e, g) (δ_H 7.348, 7.336 and 5.368 ppm) infer that one α,α′-dibromo-*p*-xylene molecule was coupled with two I3 molecules (Fig. 2). The NMR peaks of H (d, f) (δ_H 7.354, 5.377, Fig. 2) indicate that a complete coupling of one 1,3,5-tribromomethylbenzene molecule with three I3 molecules occurred. In particular, the whole norfloxacin molecular backbone could be kept safely by using inorganic/organic acids or bases, indicating that the final compounds might show dramatic acid/base tolerance. In addition, the pure final products could be easily isolated by simple washing and precipitation in ether (Not necessary to employ column chromatography or HPLC), which guaranteed us to obtain the purified target compounds at grams scale in the laboratory.

The 2D ^{1}H NMR spectra (COSY) show that the positions at (4.18, 1.52) represent the H—H of —CH_2—CH_3 in the g-position and k-position in the RLC (Fig. S1), and the h-position and l-position in the TBCs (Fig. 2), respectively. The positions located at (3.31, 2.73) show the H—H of —CH_2—CH_2— in the i- and j-positions in the RLC and the j- and k-positions in the TBCs, respectively. The positions located at (7.50, 7.39) suggest the c- and d-positions in the RLC and the d-, e-positions (H—H of —CH—CH—) in the TBCs, respectively. Hence, the COSY 2D ^{1}H NMR spectra also confirm that the target compounds were nicely prepared and isolated.

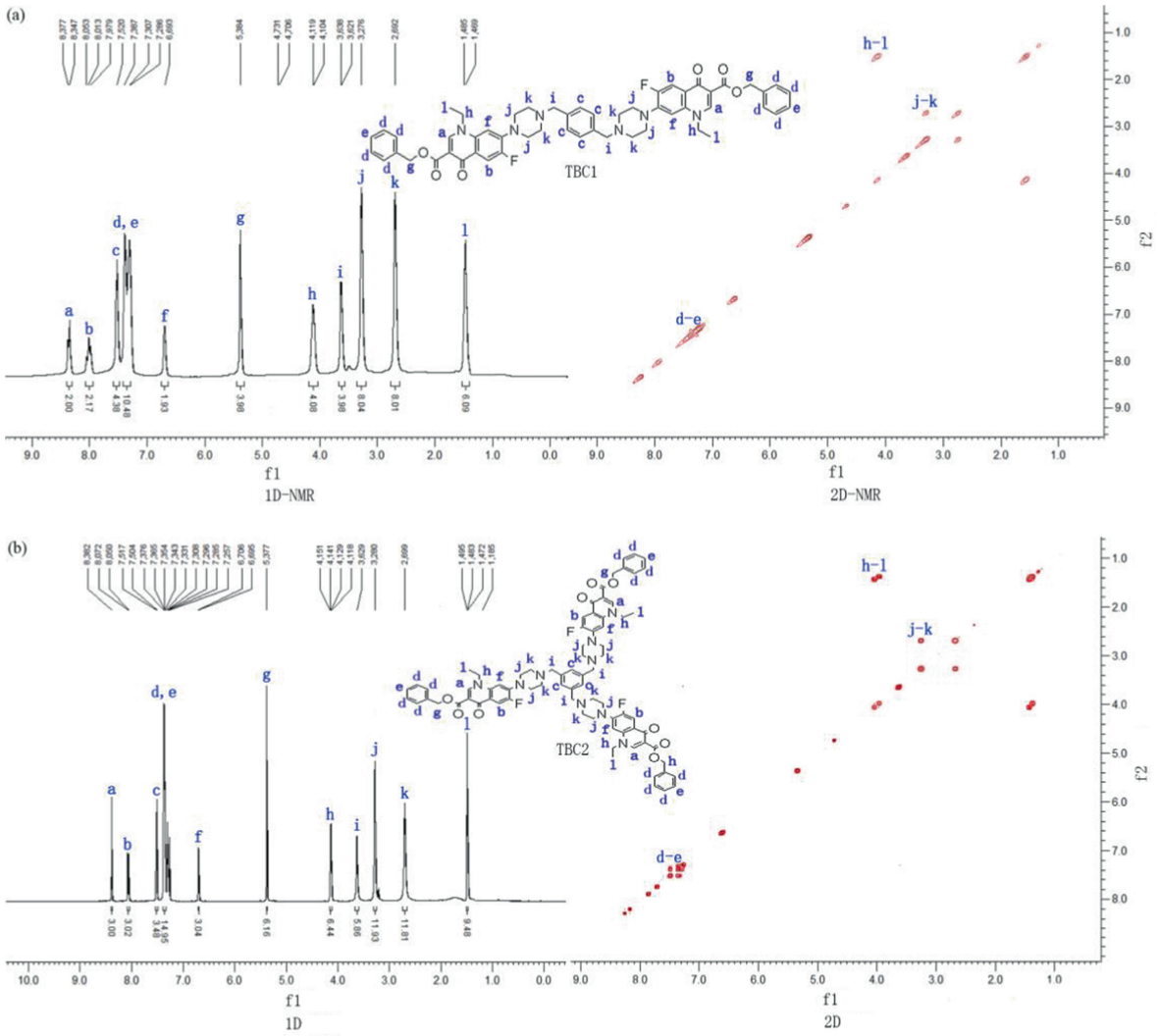

Fig. 2. The 1D and 2D COSY ^{1}H NMR spectra of the target compounds: (a) TBC1, (B) TBC2.

3.2. The adsorption of the studied compounds on mild steel surface

3.2.1. SEM micrographs

As shown in Fig. 3 and Fig. S2, the surface appearance of the mild steel surface, including the freshly polished blank steel, the polished blank steel immersed in 1.0 mol·L^{-1} HCl solution for 24 h, and the polished steel covered by the studied compounds immersed in 1.0 mol·L^{-1} HCl solution for 24 h is characterized by the SEM micro imaging. Fig. 3(a) shows the surface morphology of the newly polished mild steel is smooth with a small amount of wear marks caused by the ground. However, after the blank steel plate is immersed in 1.0 mol·L^{-1} HCl solution for 24 h, the wear scars are completely destroyed, and the steel surface is dissolved and corroded, and full of corrosion bands, peaks and spots (Fig. 3(b)).

The surface morphologies of the target compounds covered steel specimens after immersion in 1.0 mol·L^{-1} HCl solution for 24 h were also measured (Fig. 3(c)–(h)). Overall, the target compounds form tight adsorption films on the mild steel surface, and the ground marks on the polished steel surface are covered by the TBCs adsorption films. Furthermore, it is found that the best adsorption layers of the TBCs on the metal surface (the most compact and uniform films) are formed at 0.100 mmol·L^{-1}, which completely covers all the polished traces, thereby protecting the metal from the corrosion in HCl solution. It is further shown that the adsorption films of the TBCs are tighter than that of the RLC (Fig. S2), indicating the better anticorrosion effect of the TBCs layers on the mild steel plate.

3.2.2. EDS spectra

The EDS spectra of the studied mild steel surface after immersion in 1.0 mol·L^{-1} HCl solution for 24 h, uncovered and covered by the target compounds are shown in Fig. S3. As compared with the bare mild steel surface, the oxygen content of the low carbon steel surface adsorbed by the target molecules shows a sharp decrease, indicating that the corrosion products on the metal surface are reduced. The EDS spectrum shown in Fig. S3(a) suggests that no additional characteristic peaks of N and F atoms (contained in the target molecules) are found in the bare metal surface. Therefore, the results indicate that the target compounds are adsorbed on the steel surface to reduce the corrosion rate in HCl solution. In addition, it is found that the adsorption of N element on the steel surface covered by the TBCs adsorption films is more than that adsorbed by the RLC adsorption layer (comparing with Fig. S3 (b)–(d)), suggesting the stronger adsorption and better anticorrosion effects of the TBCs on mild steel.

3.2.3. AFM micrographs

Fig. 4 shows the AFM micrographs and corresponding height distribution maps of the surface of the steel sheet after immersion in 1.0 mol·L^{-1} HCl solution for 1 h, including the freshly ground

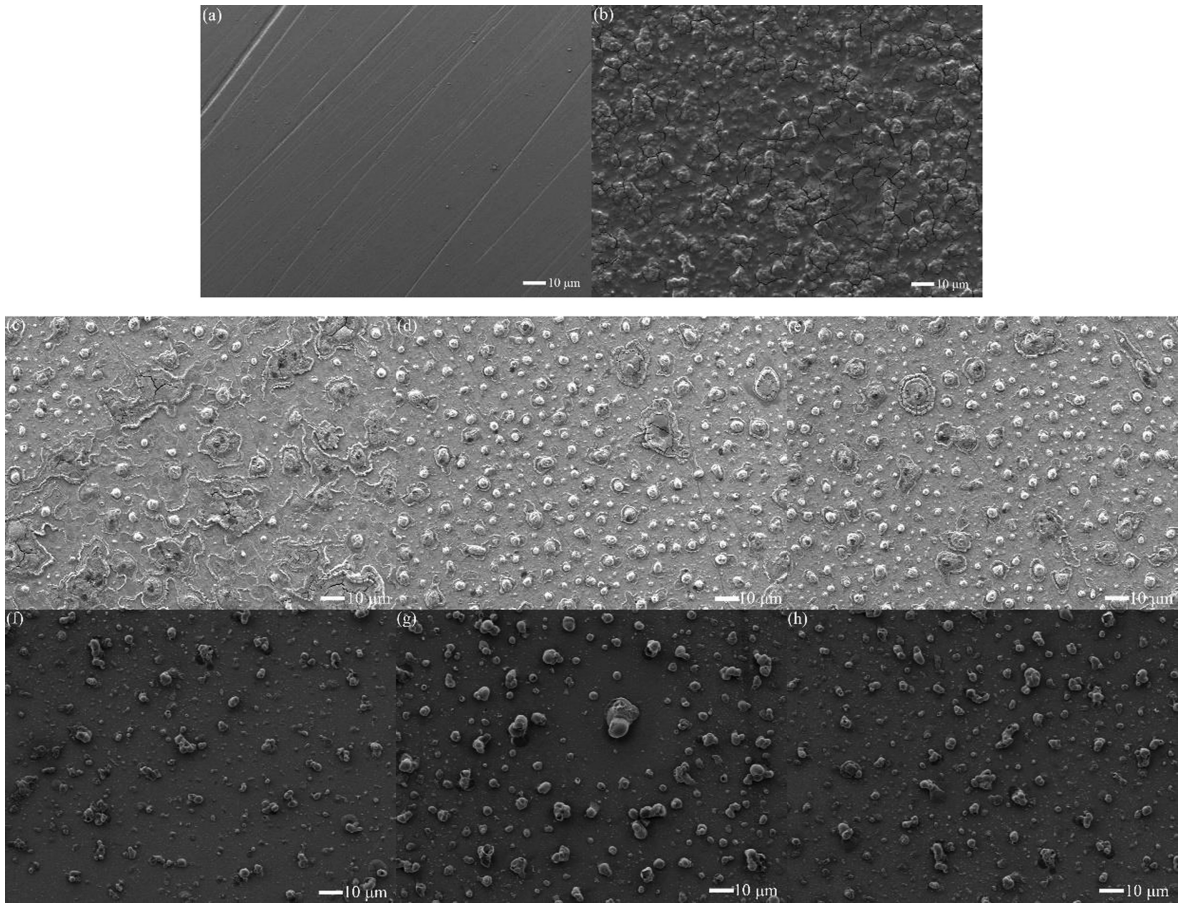

Fig. 3. SEM micrographs of mild steel surface after immersion in 1.0 mol·L^{-1} HCl solution for 24 h: (a) the newly polished steel specimen, (b) the bare polished steel specimen after immersion, (c)–(e) the polished steel specimens covered by the TBC1 of various concentrations (0.100, 0.150 and 0.200 mmol·L^{-1}) after immersion, (f)–(h) the polished steel specimens covered by the TBC2 of various concentrations (0.100, 0.150 and 0.200 mmol·L^{-1}) after immersion.

blank steel plate and the steel plates adsorbed by the TBCs. Fig. 4(a) shows that the surface of the polished mild steel plate is relatively smooth, and its average roughness is only 5.706 nm. On the contrary, Fig. 4(c) suggests that the blank mild steel plate surface is corroded severely in acid solution, and a rough structure with huge pits and peaks are observed, and the average roughness reaches 61.106 nm.

Fig. 4(e)–(h) suggest the atomic force three-dimensional structure and corresponding height distribution maps of the steel samples covered by the adsorption layers of the TBCs after immersion in HCl solution. It is shown that the surface of the steel sheet is kept relatively smoothly, and the corresponding average roughness values are around 10 nm. Besides, the corresponding height distribution map gives a quite flat curve with height fluctuations only within 50 nm. This indicates that the TBCs adsorption layers can effectively prevent from the corrosion of mild steel surface in acid medium. The AFM microscopy also suggests that the steel surface covered by the TBCs (Fig. 4(e), (g)) is flatter than that adsorbed by the RLC (Fig. S4), reflecting that the adsorption films of the TBCs on the steel plate are more compact. Therefore, a more pronounced preservative effect of the TBCs adsorption films may be achieved.

3.2.4. The XPS spectroscopy

The TBCs adsorbed on surface of the mild steel sheet was analyzed by the XPS spectroscopy to further study the adsorption mechanisms. Figs. 5–8 show the XPS spectra of Fe, C, O, N elements on the studied steel sheet surface. The steel samples covered by the TBCs was soaked in 1.0 mol·L^{-1} HCl solution for 1 h, and the blank steel sample was also included in 1.0 mol·L^{-1} HCl solution for 1 h as a reference control.

Fig. 5 shows the Fe $2p_{3/2}$ XPS of the studied blank steel sheet (Fig. 5(a)), the steel sheet covered by the TBC1 (Fig. 5(b)) and TBC2 (Fig. 5(c)). Table S1 lists the corresponding resolved parameters of Fe $2p_{3/2}$ XPS. Besides, the Fe $2p_{3/2}$ XPS spectroscopy and the corresponding resolved parameters of the mild steel plates covered by the RLC are shown in Fig. S5 and Table S1.

The Fe $2p_{3/2}$ XPS spectrum of the blank steel sheet shows that the peak fittings are located at Fe_2O_3/Fe_3O_4 (710.44 eV), FeOOH (712.15 eV) and $FeCl_3$ (715.23 eV). The Fe $2p_{3/2}$ XPS spectra of the steel sheets adsorbed by the TBCs are divided into the three convolution peaks. For example, to the TBC1, Fe^0 (706.43 eV), Fe_2O_3/Fe_3O_4 (710.00 eV) and FeOOH (712.33 eV), and to the TBC2, Fe^0 (706.47 eV), Fe_2O_3/Fe_3O_4 (709.89 eV) and FeOOH (711.80 eV) [16]. The above results show that both the blank sample and the steel plate adsorbed by the TBCs have the XPS signals of Fe^{3+} and Fe^{2+}. However, Fe^0 signal is found on the mild steel plate surface covered by the TBCs. The results indicate that the TBCs adsorption layers on the mild steel plate surface can effectively inhibit the oxidation of iron, showing the excellent anticorrosion performance.

Fig. 6 shows the C 1s XPS spectra of the studied steel surface, and the corresponding parameters are shown in Table S2. The resolved C 1s XPS spectrum and parameters of the steel surface covered by the RLC are given at Fig. S6 and Table S2. The C 1s

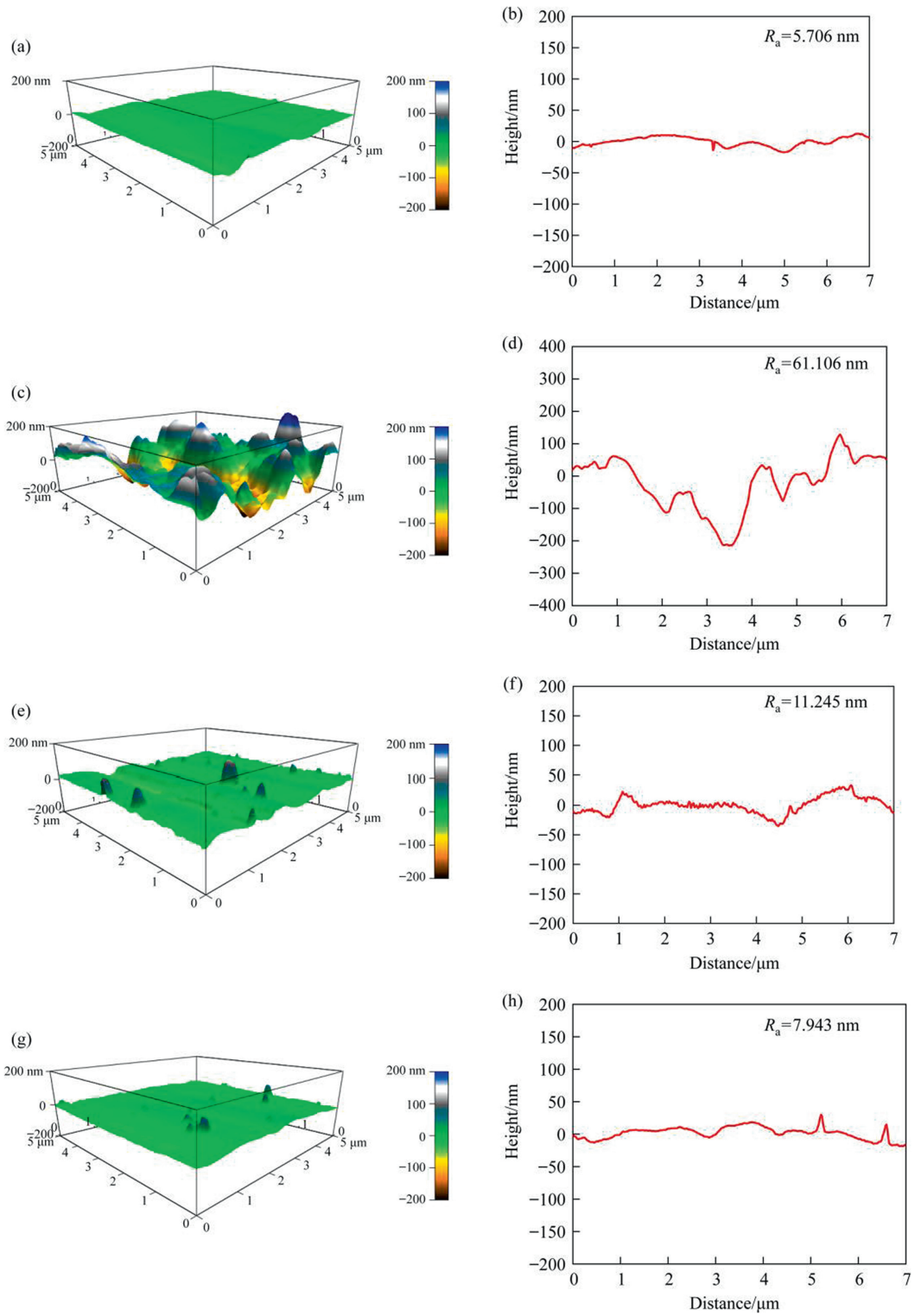

Fig. 4. AFM micrographs of the studied freshly polished mild steel specimen after soaked in 1.0 mol·L^{-1} HCl solution for 60 min: (a) the studied freshly polished mild steel specimen, (c) the studied polished mild steel specimen after the soaking, (e) the studied polished mild steel specimen surface covered by the TBC1 after the soaking, (g) the studied polished mild steel specimen surface covered by the TBC2 after the soaking, and (b), (d), (f), (h) are the corresponding height profile graphs of to (a), (c), (e), (g), respectively (the adsorption time, 8 h, at 0.150 mmol·L^{-1}).

XPS spectrum of the blank steel sheet shown in Fig. 6(a) is fitted to the three deconvoluted peaks at 285.00 eV, 286.41 eV and 289.62 eV, corresponding to the characteristic peaks of C—C/C=C, C—O and C=O, respectively [17]. These peaks can be yielded by the carbon contamination in the air [18]. While, the C 1s spectra of the mild steel plate surface adsorbed by the TBCs contain the four deconvoluted peaks, which suggests that the four chemical forms of carbon are found on the surface of the steel sheets. The main peak at 285.11 eV in the C 1s XPS spectrum XPS spectrum of the mild steel covered by the TBC1 is mainly due to the contam-

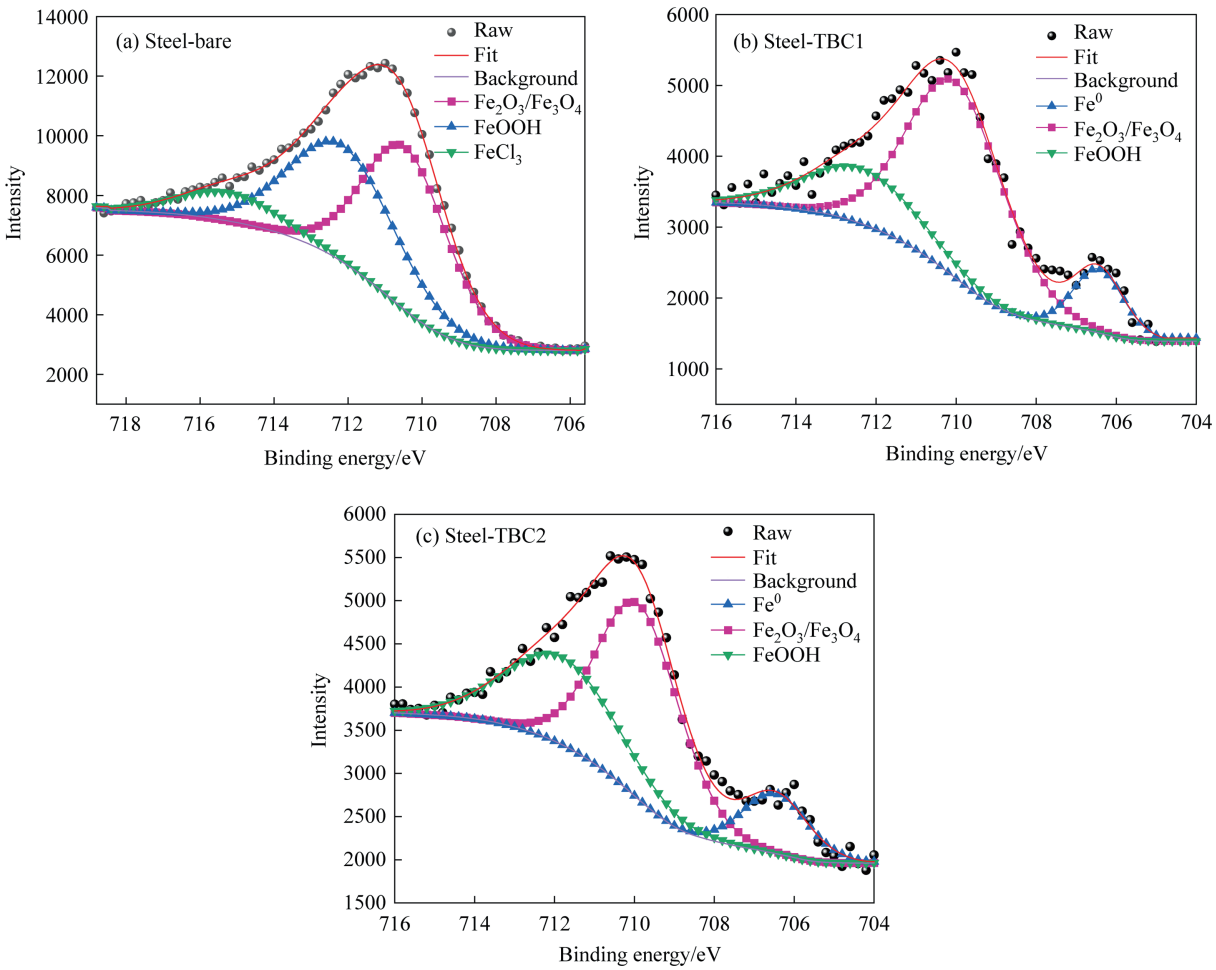

Fig. 5. (a) Fe $2p_{3/2}$ XPS spectra acquired from investigated blank steel surface, and Fe $2p_{3/2}$ XPS spectra obtained from studied steel specimens adsorbed by (b) the TBC1 and (c) the TBC2, after incubated in HCl solution for 60 min.

ination of hydrocarbons and the C—C/C=C bond contained inside the TBC1 (Fig. 6(b)). The other three peaks are located at 286.73 eV, 288.38 eV and 289.37 eV, corresponding to the characteristic peaks of C—O, C—N and C=O, respectively. Fig. 6(c) is the C 1s XPS spectrum of the TBC2 covered mild steel surface. The main peak at 285.02 eV is mainly due to the contamination of hydrocarbons and the C—C/C=C bond contained inside the TBC2. The other three peaks are located at 286.66 eV, 287.73 eV and 289.05 eV, corresponding to the characteristic peaks of C—O, C—N and C=O, respectively. It is found that the C 1s XPS spectra of the TBCs adsorbed steel sheets show more obvious C—O, C=O and C—N peak as compared to those of the RLCs covered steel sheet, indicating that the target compounds are adsorbed on the steel sheet surface more efficiently.

Fig. 7 shows the O 1s XPS energy level spectra of the blank steel sheet and the steel sheets adsorbed by the TBCs, and the corresponding parameters are listed in Table S3. The O 1s XPS energy level spectrum of the steel sheet adsorbed by the RLC is presented in Fig. S7. Fig. 7(a) shows the O 1s XPS energy level spectrum of the blank steel sheet, which can be divided into the two deconvolution peaks of Fe_2O_3/Fe_3O_4 and FeOOH at 529.25 eV and 530.92 eV, respectively [19]. However, the O 1s XPS energy level spectrum of the mild steel samples covered by the TBCs can be divided into three convolution peaks, namely Fe_2O_3/Fe_3O_4, FeOOH and C—O/C=O (Fig. 7(b), (c)), for example to the TBC1, 529.39 eV, 530.82 eV, 531.51 eV, TBC2, 531.47 eV, 529.76 eV, 529.16 eV). The existence of C—O/C=O also confirms that the target branched compounds are adsorbed on the surface of mild steel plates. And it is shown that the C—O/C=O peak of the TBC2 covered steel plate displays the largest intensity, indicating the greatest and tightest adsorption film on the mild steel specimen.

Fig. 8 shows the N 1s XPS energy level spectra of the TBCs adsorbed on the steel surface. The corresponding parameters are shown in Table S4. The XPS energy level spectrum of N 1s on the steel surface covered by the RLC is shown in Fig. S8. The XPS energy levels of the steel samples confirm the two chemical environments of N 1s, including C—N and N—Fe. The peaks at 399.04 eV and 399.36 eV are the characteristic peaks of the C—N group, which can be generated by the target compounds [20]. The N 1s energy level peaks at 400.44 eV and 400.67 eV may be the characteristic peaks of the N-Fe complex, which indicates that nitrogen atoms in the target compounds can coordinate with iron atoms to drive the adsorption on mild steel surface [21].

3.2.5. X-ray diffraction (XRD) spectroscopy

Fig. 9 shows the X-ray diffraction spectroscopy of the mild steel plate adsorbed by the TBCs and the blank mild steel plate after immersion in 1.0 mol·L^{-1} HCl solution for 30 min. It is shown that the X-ray diffraction pattern of blank steel sheet (steel-bare) has the three peaks located at 11.5° (FeOOH), 22.6° (FeOOH) and 33.7° (Fe_3O_4) [22]. This can be attributed to the corrosion of steel producing oxides and hydroxides. The other three peaks are Fe^0 peaks (45.0°, 65.5°, 82.8°) [23]. However, only the three Fe^0 peaks remain on the surface of mild steel sheets adsorbed by the TBCs,

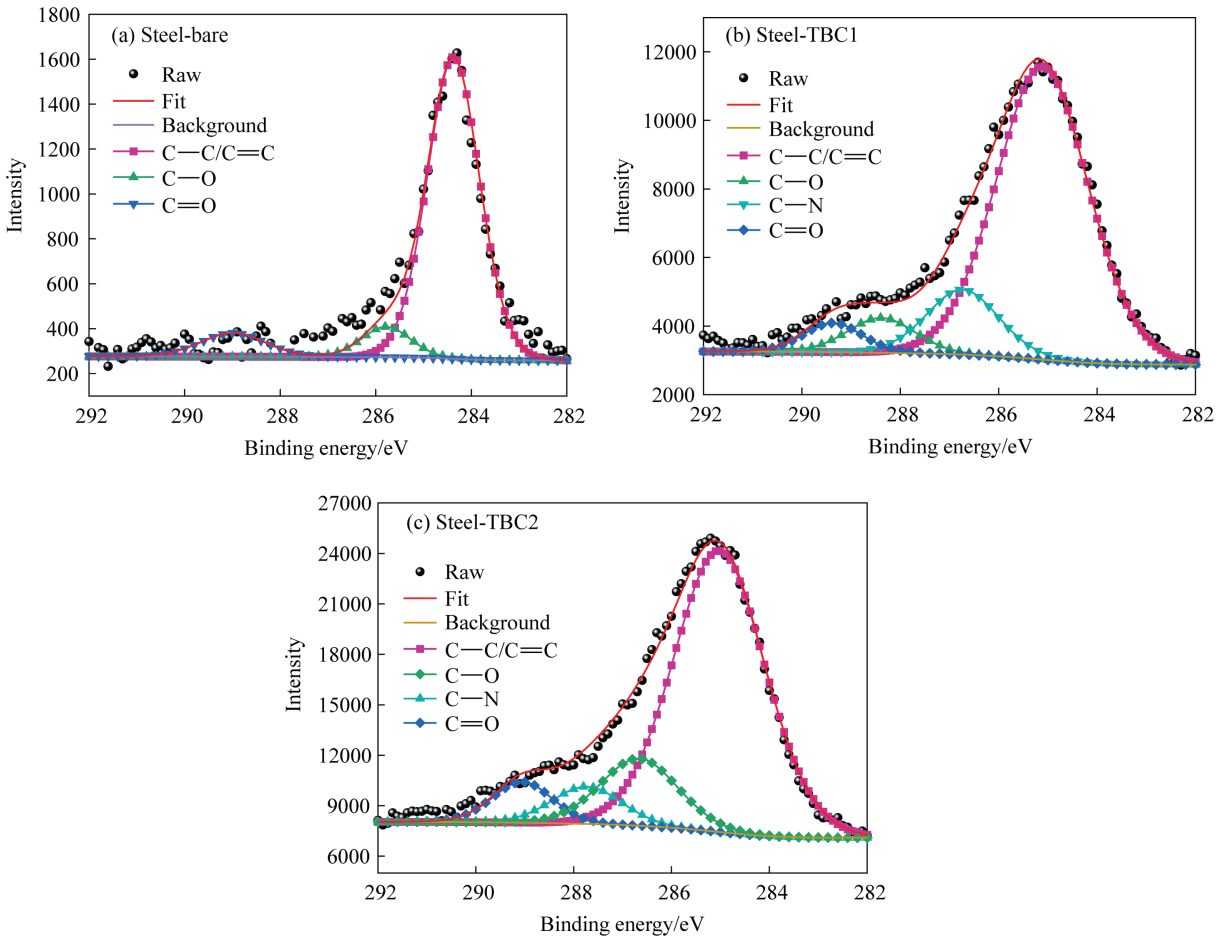

Fig. 6. (a) C 1s XPS spectra obtained from the investigated bare steel surface, (b) C 1s XPS spectra yielded from the studied mild steel specimens absorbed by the TBC1, (c) C 1s XPS spectra yielded from the studied mild steel specimens absorbed by the TBC2, after the metal samples immersed in HCl solution for 60 min, respectively.

indicating that the adsorption films of the target branched molecules can inhibit the corrosion of steel in hydrochloric acid medium. In contrast, the X-ray diffraction pattern of the RLC-adsorbed mild steel sheet shows the four peaks, including Fe^0 peaks (45.3°, 65.4°, 82.5°) and a FeOOH peak at 11.5°. Hence, the X-ray diffraction pattern shows that the corrosion inhibition effect of the target branched compounds is more remarkable than that of the reference linear molecule.

3.3. Electrochemistry analysis

3.3.1. Polarization curves

Fig. S9 shows the open circuit potential-time relationships of the blank steel electrodes obtained in 1.0 mol·L^{-1} HCl solution and the steel electrodes adsorbed by different concentrations of the TBCs, and the corresponding dynamic potential electrodes are shown in Fig. 10. The Tafel curve of steel sheet adsorbed by the RLC is located in Fig. S10. The results show that the above electrodes display similar electrochemical mechanisms, which are composed of oxidation reaction at the anode branch (mainly the process of losing electrons) and reduction reaction (the process of gaining electrons) at the cathode branch. The electrochemical parameters (corrosion potential (E_{corr}), corrosion current density (I_{corr}), corrosion rate (CR), Tafel cathodic slope (β_c), Tafel anodic slope (β_a) and corrosion inhibition efficiency (η_j) obtained from the polarization curves are listed in Table S5.

It is shown that the cathode branches in the Tafel curves the steel electrodes adsorbed by the TBCs are located at a lower position on the vertical axis, and the corrosion current density I_{corr} values are significantly lower than that of the blank steel electrode. The decreasing trend is more dramatic with increasing the concentrations of the TBCs from 0.010 mmol·L^{-1} to 0.150 mmol·L^{-1}. This phenomenon can be explained by the increase of the adsorption amounts and the coverage areas of the TBCs on the steel surface, which may block the metal dissolution in the active zone more effectively.

Seen from Fig. 10, the positive and negative parts in the Tafel curves of the TBCs adsorbed electrode move to negative potentials with respect to the zero-charge potential, indicating that the TBCs adsorption layers on the working steel electrodes can inhibit the cathodic and anodic redox processes, thereby preventing the mild steel from being damaged in corrosive acid solution. The polarization results suggest a mixed anodic and cathodic inhibitory mechanism [24,25].

The cathodic branches follow the same pattern in all the samples, demonstrating the cathodic inhibition of the mild steel electrode surface covered by the TBCs in acid solution [26]. In addition, the invariant hydrogen evolution reaction mechanism in the cathode region can be further inferred by observing the parallel branches. The cathodic protection performance is more remarkable, but the anodic protection cannot be negated [27]. As can be seen from the polarization curves, the anode branch is also affected by the adsorption of the target molecules on the working

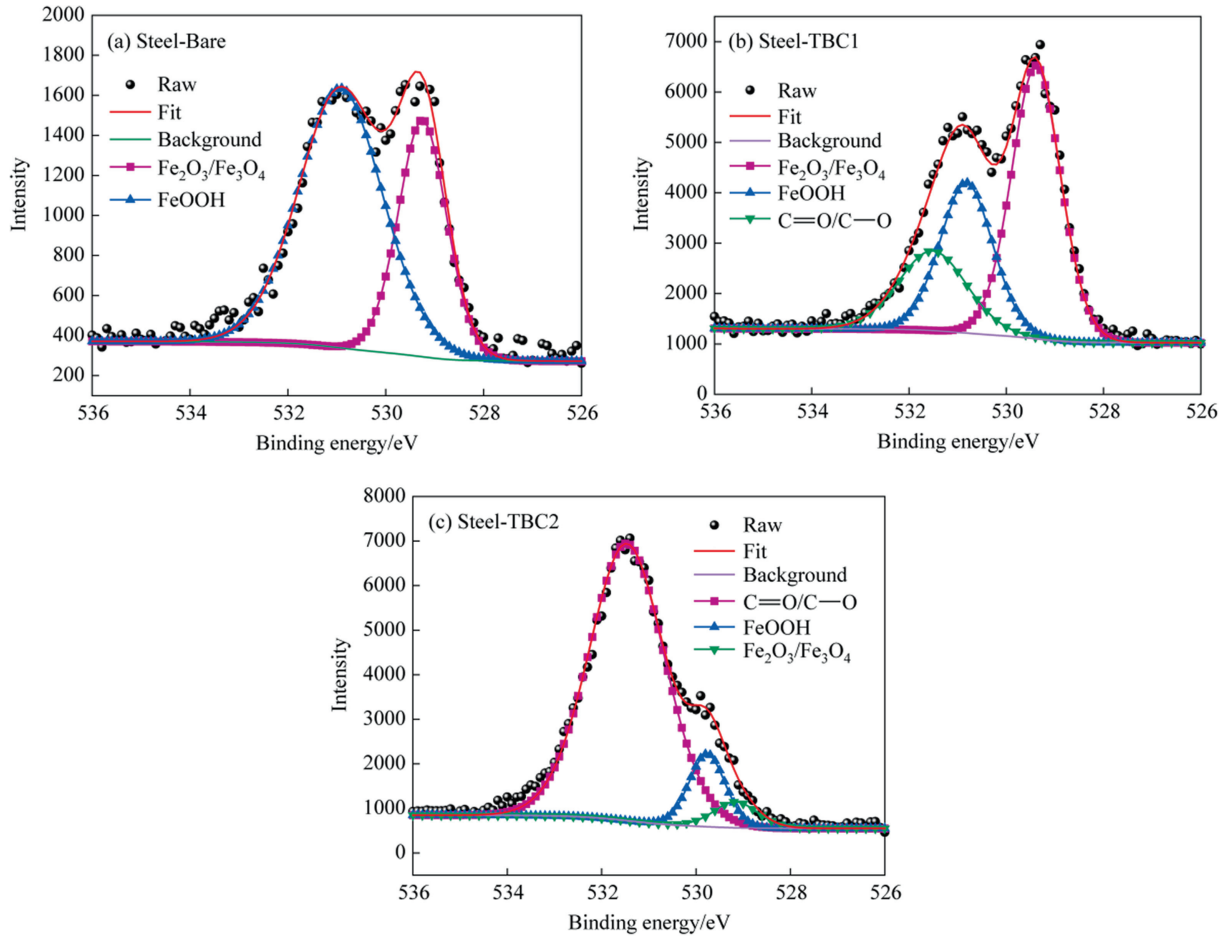

Fig. 7. (a) O 1s XPS spectra detected from investigated bare steel surface, (b) O 1s XPS spectra from surveyed steel specimen surface treated by the TBC1, (c) O 1s XPS spectra from surveyed steel specimen surface treated by the TBC2, after the metal samples immersed in HCl solution for 60 min, respectively.

mild steel electrodes. Therefore, the target compounds show both cathodic and anodic protection for mild steel in acid medium [28]. But to a certain extent, since the displacement in the cathodic direction is larger than that in the anodic direction, it can be deduced that the inhibition of the cathodic reactions of the steel electrodes covered by the TBCs is more prominent.

Table S5 shows that the values of I_{corr} decrease with the increase of the TBCs concentrations in a range of 0.010–0.150 mmol·L^{-1}, and reach a minimum value at 0.150 mmol·L^{-1}. Furthermore, the corrosion inhibition efficiencies (η_j) arrive at a maximum value at 0.150 mmol·L^{-1}. While as the concentration is at 0.200 mmol·L^{-1}, the corrosion inhibition efficiencies show a downward trend. It suggests that the adsorption films of the TBCs on the steel working electrodes can be looser at the concentration of 0.200 mmol·L^{-1}. Moreover, the E_{corr} exhibits a similar change tendency as the I_{corr}, which moves to the negative direction with an increase of the concentrations of the TBCs. This phenomenon further confirms that the anticorrosion effect of the TBCs adsorption layers on mild steel in hydrochloric acid medium is mainly achieved by preventing from the cathodic electrode reaction [29].

The slope values of the Tafel curves (β_a, β_c) obtained at different concentrations are similar, further indicating that the corrosion reaction mechanism is not changed by the concentrations of the TBCs. To the adsorbed working electrode, if the negative value of E_{corr} is less than 85 mV as compared with the corresponding blank electrode, it is consistent with the mixed-type cathodic and anodic mechanism. It can be further seen from Table S5 that the deviations of the E_{corr} values of the steel electrodes covered by the studied compounds as compared with the blank electrodes are all within 85 mV.

Therefore, the studied molecules can be regarded as mixed-type corrosion inhibitors [30], which can be adsorbed on the active sites of metallic steel surface, thereby reducing the anodic metal dissolution and cathodic hydrogen evolution reaction, thus inhibiting the electrochemical reaction [31]. Meanwhile, the variations of corrosion current density are caused by the adsorption films of the TBCs and RLC on the steel sheet surface.

3.3.2. Electrochemical impedance spectroscopy (EIS)

The corrosion inhibition effect of different concentrations of the studied molecules on mild steel in HCl medium was further determined by electrochemical impedance spectroscopy (EIS). The Nyquist curves and Bode plots of the blank steel electrodes and the steel electrodes covered by the TBCs are shown in Fig. 11(a)–(d). The Nyquist and Bode curves of the RLC covered steel electrode are shown in Fig. S11.

To the EIS spectrum of blank mild steel electrode in acid solution, the equivalent circuit shown in Fig. 12(a) can be used for the fitting the plots, herein R_s means the resistance of solution between working electrodes and reference electrons, R_{ct} is the resistance of charge transfer, R_f is the resistance of pore solution. Besides, the constant phase element CPE_f consists of membrane capacitance C_f and deviation parameter n_1, and the CPE_{dl} comprises double-layer capacitance C_{dl} and deviation parameter n_2. As shown in Fig. 11, the Nyquist curves of the TBC1 covered steel electrode consist of a single capacitive arc, which is a concave semicircle

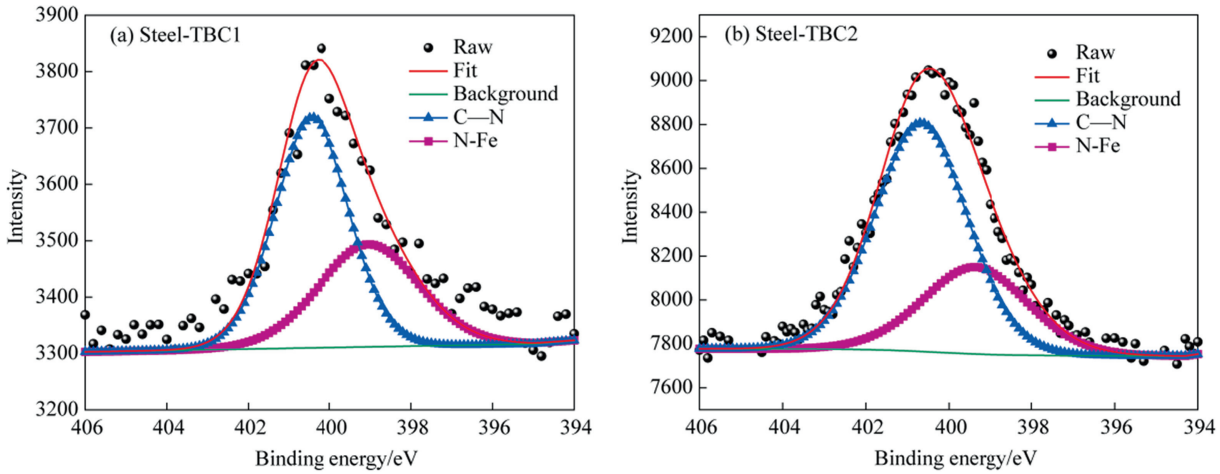

Fig. 8. (a) N 1s XPS spectra from surveyed steel specimen surface treated by the TBC1, (b) N 1s XPS spectra from surveyed steel specimen surface treated by the TBC2, after the metal samples immersed in HCl solution for 60 min, respectively.

formed by charge-transfer resistance and double-layer capacitance. It can be fitted with the equivalent circuit shown in Fig. 12 (b), where R_f is the pore solution resistance.

It can be seen in Fig. 11 that as the imaginary impedance value exceeds 2000, a straight line at 45° to the coordinate axis appears on the impedance complex plane graph, and a diffusion tail appears in the Nyquist graphs, indicating that the electrochemical process is controlled by the activation of the concentration polarization. This is the Warburg impedance that occurs due to the diffusion-induced concentration polarization.

The equivalent circuit shown in Fig. 12(c) can be used for the fitting the Nyquist plots as well. The reason for this phenomenon may be that at the higher concentrations of the adsorbed target molecules, the Nyquist diagrams contain the Warburg impedance due to the simultaneous existence of charge transfer control and diffusion control in the acid solution. While at the lower concentrations, mainly owing to the charge transfer control, this phenomenon occurs when the ratio of the both is equal at high concentrations [32]. The corresponding equivalent circuit diagrams R(Q(RO)), R(Q(R(Q(R)))), (R(Q(R(Q(RW))))) are fitted by the ZSimpWin software. The EIS plots of the RLC covered steel electrode that are given in Fig. S11 suggest that there is absence of Warburg impedance phenomenon, probably because the charge transfer control is more competitive.

The results show that the capacitive arc of the steel electrode adsorbed by the TBCs increases with the increasing concentrations of the adsorbed TBCs in a range of 0.010–0.150 mmol·L^{-1}, meaning the corrosion inhibition of the steel electrodes is enhanced. The capacitive arc decreases as the concentration continues to increase until 0.200 mmol·L^{-1}. This indicates that the adsorption capacity of the TBCs on the surface of the working electrode becomes weaker at 0.200 mmol·L^{-1}. Therefore, the corrosion resistance of the steel electrodes is also weakened accordingly at 0.200 mmol·L^{-1} of the TBCs.

The Bode plots show that as the TBCs concentrations increase from 0.010 mmol·L^{-1} to 0.150 mmol·L^{-1}, the impedance values increase over the defined frequency range, reaching the maximum at 0.150 mmol·L^{-1}. Likely, the maximum phase angle values increase with the increasing concentrations of the TBCs (0.010–0.150 mmol·L^{-1}). However, the impedance value and phase angle value of the steel electrodes adsorbed by the TBCs of 0.200 mmol·L^{-1} show a decrease. Furthermore, it is noted that the magnitude of the charge transfer impedances and the magnitude of the phase angles (Fig. 11(b), (d)) also display the same trend as the capacitive arc radius. With the increase of the TBCs' concentrations, the charge transfer resistance gradually increases, and the phase angle gradually increases. The maximum phase angle regions of the adsorbed TBCs steel electrodes are wider than that of the blank steel electrode.

The obtained electrochemical parameters are listed in Table S6. Furthermore, the smaller χ^2 values reflect the rationale equivalent circuit diagrams. The R_s values represent the impedance of the electrolyte solution; R_{ct} shows the charge transfer resistance; R_p is the pore solution resistance; and W stands for the Warburg impedance. In addition, the constant phase element CPE_f includes the membrane capacitance C_f and the dispersion effect index n_1, and CPE_{dl} includes the double layer capacitance C_{dl} and the dispersion effect index n_2. The Z_{CPE} and C_{dl} values can be obtained from the CPE parameters Y and n from Eqs. (3) and (4) [33–35].

$$Z_{CPE} = \frac{1}{Y(j\omega)^n} \tag{3}$$

$$C_{dl} = Y_0(\omega)^{n-1} = Y_0\left(2\pi f_{Z_{im-Max}}\right)^{n-1} \tag{4}$$

Herein, Y_0 means the admittance of electrochemical system, j represents the imaginary root, ω shows the angular frequency, n is the deviation parameter ascribed to phase shift. $f_{Z_{im-Max}}$ is the frequency at the peak imaginary part in a Nyquist curve.

As shown in Table S6, the R_{ct} and R_{pore} values obtained by fitting the corresponding equivalent circuit diagrams increase with increasing the concentrations in a range of 0.050–0.150 mmol·L^{-1}. This may be due to the corrosion inhibition effect of the TBCs adsorbed on the working steel electrodes. However, the double-layer capacitances C_f and C_{dl} decrease significantly in a concentration range of 0.010–0.150 mmol·L^{-1} as compared with the blank electrode due to the adsorption of the TBCs on the steel surface. The possible reason for this phenomenon is that the thickness of the protective layer increases with the increase of the adsorption amounts of the TBCs, so that the adsorption of the TBCs reduces the contact surface of water molecules and aggresive ions with the metal surface. Therefore, the corrosion inhibition efficiencies η_i value defined by the charge transfer resistance can reach a maximum value at 0.150 mmol·L^{-1}.

However, the corrosion inhibition efficiencies of the TBCs decrease as the concentrations further increase till 0.200 mmol·L^{-1}. The fitting parameter n is between 0.7 and 1.0, indicating that the equivalent circuit may well describe the charge transfer process of

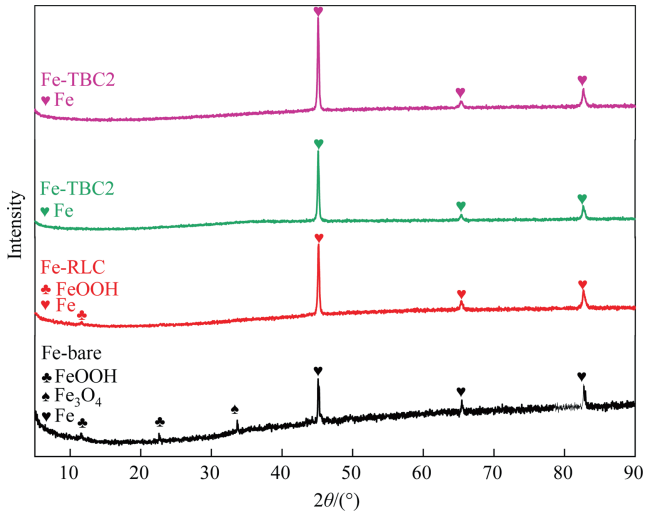

Fig. 9. XRD patterns of corroded blank steel surface and corroded steel samples adsorbed by the studied molecules (0.150 mmol·L^{-1}) (after immersion in acid solution for 1 h).

metal corrosion. The small error values χ^2 suggest that the equivalent circuit fitting results are consistent with the actual process of electrode corrosion in acid solution [36]. Combined with the EIS results of the steel electrode covered by the RLC (Table S6), it can be seen that the change tendency of its corrosion inhibition efficiencies with the concentration changes is consistent with those of the TBCs. But its maximum corrosion inhibition efficiency (87.80%) is much lower than that of TBC1 (97.93%) and TBC2 (98.35%), which may be related to the different molecular structures.

3.3.3. Adsorption isotherms plots

The adsorption isotherms were studied to verify the adsorption of the studied compounds on mild steel substrates. Thus, Langmuir [37], Temkin [38], Frumkin [39] and Freundlich [40] models are employed to fit the experimental results. A very close 1.00 of R^2 suggest that the most reasonable fitting could follow the Langmuir isotherm (Eq. (5)) [41,42].

$$\frac{c}{\theta} = \frac{1}{K_{ads}} + c \tag{5}$$

Herein, K_{ads} shows the adsorption equilibrium constant, and c is the concentration of the studied compounds.

Fig. S12 suggests that the Langmuir model is reasonable, and the standard adsorption free energy changes can be obtained by the following Eq. (6) [43]:

$$\Delta G^0_{ads} = -RT \ln (55.55 \times K_{ads}) \tag{6}$$

wherein R shows the molar gas constant (8.314 J·mol^{-1}·K^{-1}), T is the absolute temperature (298.15 K).

Fig. S12 and Table S7 show the adsorption isotherms and thermodynamic parameters of the TBCs and RLC on mild steel surface. The linear correlation coefficients R^2 of the adsorption isotherms of the TBCs on the surface of mild steel are both 0.9999, demonstrating that the TBCs can be adsorbed to the metal surface to form protective layers for inhibiting the dissolution of metal in hydrochloric acid solution.

The negative ΔG^0_{ads} indicates that the adsorption of TBCs on the mild steel surface is a spontaneous process. As the absolute value of ΔG^0_{ads} is equal to or less than 20 kJ·mol^{-1}, the organic molecules act on the metal surface through physisorption, which can be caused by electrostatic interaction and van der Waals force. While the absolute value of ΔG^0_{ads} is equal to or greater than 40 kJ·mol^{-1}, it indicates that an organic molecule is adsorbed on the metal surface with a chemisorption, that is, this compound transfers electrons to the metal surface to form chemical coordination bonds [44,45].

It is found that the absolute values of ΔG^0_{ads} of the TBCs are greater than 40 kJ·mol^{-1} (40.98 kJ·mol^{-1}, 41.89 kJ·mol^{-1}), suggesting that the studied molecules display strengthened chemisorption on the mild steel surface. In contrast, the absolute value of ΔG^0_{ads} of the RLC between 20–40 kJ·mol^{-1} reflects the occurrence of both physisorption and chemisorption on mild steel surface.

3.4. Molecular modelling

The optimized structures, frontier orbital density distributions and Mulliken charges and the associated quantum chemical parameters of the RLC, TBCs are shown in Figs. S13, S14 and Tables S8, S9. Fig. S14(a) shows that the highest occupied orbital energy level E_{HOMO} and the lowest occupied orbital energy level E_{LUMO} of the TBCs are almost concentrated on the quinolone backbone, but they are not distributed on the phenyl rings linkers. It indicates that the quinolone ring and the benzene ring in the planar struc-

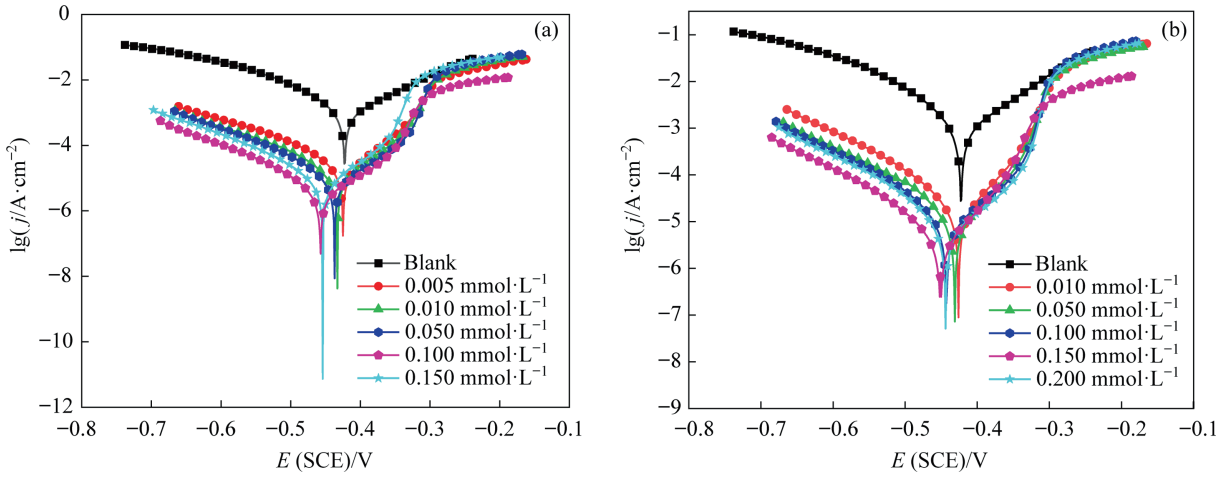

Fig. 10. (a) Tafel curves for blank mild steel electrodes and mild steel electrodes covered by the TBC1 in 1.0 mol·L^{-1} HCl solution, (b) Tafel curves for the mild steel electrodes adsorbed by the TBC2 in 1.0 mol·L^{-1} HCl solution.

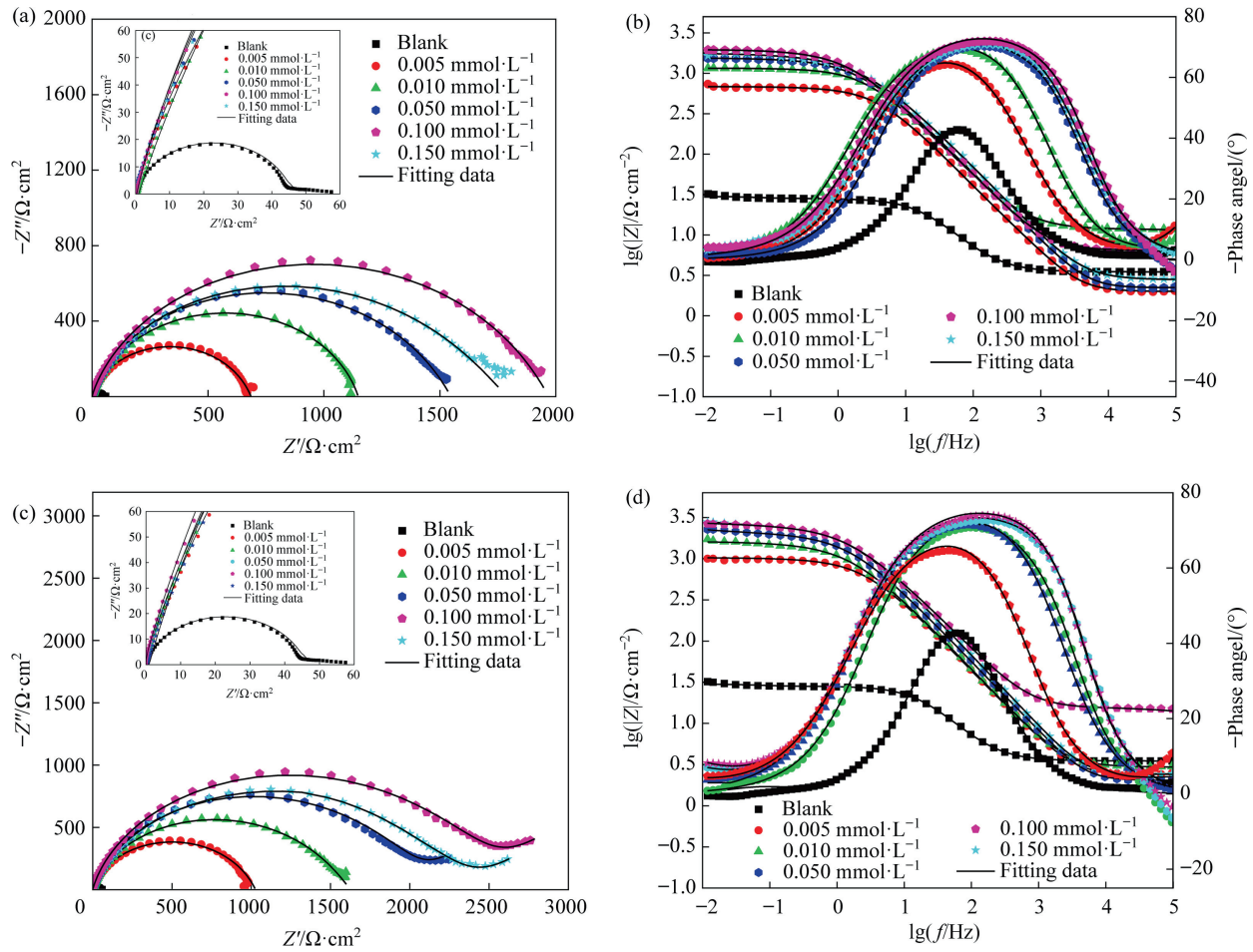

Fig. 11. Nyquist diagrams (a), (c), Bode plots (b), (d) in 1.0 mol·L^{-1} HCl solution for the studied naked mild steel electrodes, and the metal surface covered by the TBC1 (a), (b) and TBC2 (c), (d) of different concentrations.

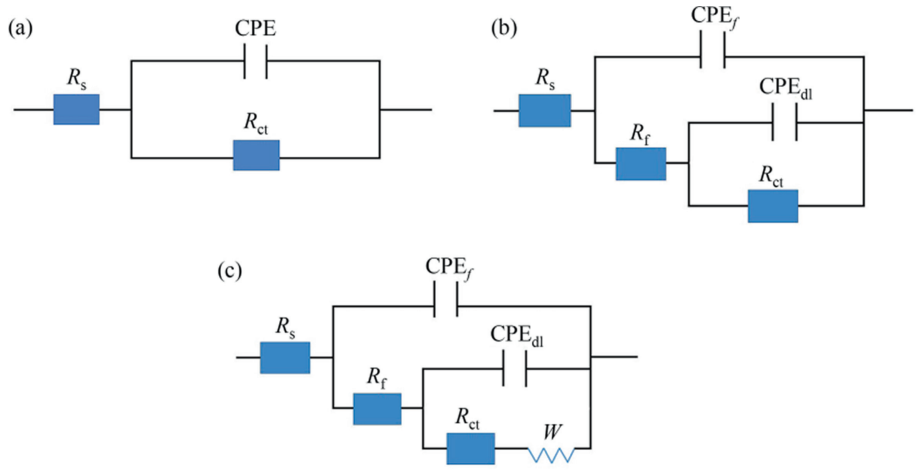

Fig. 12. Equivalent circuit models fitting EIS experimental data for (a) blank metal sample and (b), (c) the TBCs covered metal sample in this study, R_s means the resistance of solution between working electrodes and reference electrons, R_{ct} is the resistance of charge transfer, R_f is the resistance of pore solution. CPE_f represents the constant phase element, C_f is membrane capacitance, n_1 is deviation parameter, C_{dl} shows double-layer capacitance, n_2 is deviation parameter.

ture can not only donate electrons to form coordination bonds with metal ions, but also accept metal electron pairs to form feedback bonds [46].

The E_{HOMO} value is related to the electron donating ability of an organic molecule. The larger the value is, the more unstable the electrons are and the easier it is to donate electrons. The E_{LUMO} value represents the electronic property of an organic matter to accept other compounds containing lone pair electrons. The lower the value is, the easier it is to obtain electrons from the metal surface. In addition, the energy gap (ΔE) is an important parameter

that can be an indication of the interaction ability of an organic molecule with metal atoms and shows that the compound is easily adsorbed on metal surface to form an adsorption protective layer [15]. The lower the value of ΔE is, the higher stability for the formed complex is. Combined with the Tables S8 and S9, notably, the ΔE values (TBC1, 0.1329 eV, TBC2, 0.1148 eV) of the TBCs are lower than that the RLC (0.1689 eV), which reflects the stronger chemical chelation of TBCs with metallic substrate than that of RLC. This may be due to the increase numbers of norfloxacin skeletons, which leads to the more rigid and symmetrical geometry of the TBCs.

The structural parameters of the studied molecules can be obtained through quantum chemical calculation (Tables S8 and S9), including the highest occupied molecular orbital energy (E_{HOMO}), the lowest occupied molecular orbital energy (E_{LUMO}), the energy level difference ($\Delta E = E_{LUMO} - E_{HOMO}$), the electronegativity (χ), the hardness (η), softness (σ) and charge transfer fraction (ΔN), dipole moment (μ).

The values of χ, η, σ, ΔN are obtained by the following Eqs. (7)–(10) [47]:

$$\eta = -\frac{1}{2}(E_{HOMO} - E_{LUME}) \tag{7}$$

$$\chi = -\frac{1}{2}(E_{HOMO} + E_{LUME}) \tag{8}$$

$$\sigma = \frac{1}{\eta} \tag{9}$$

$$\Delta N = \frac{\chi_{Fe} - \chi_i}{2(\eta_{Fe} + \eta_i)} \tag{10}$$

wherein χ_{Fe} and η_{Fe} show the absolute subversion and absolute hardness of iron, χ_i and η_i represent the absolute subversion and absolute hardness of the organic molecules. In order to obtain the ΔN values, we adopt the theoretical values of χ_{Fe} = 7.0 eV and χ_{Fe} = 0 by assuming that for a metallic bulk $-E_{HOMO} = -E_{LUMO}$ since they are softer than the neutral metallic atoms [48,49]. Thus, the quantum chemical parameters of the studied compounds are in Table S8.

The electronegativity (χ) is the ability of an element's atoms to attract covalently bonded electron pairs [50]. It can be seen that the electronegativity of TBC2 is generally greater than that of TBC1 and RLC. This shows that TBC2 molecules are easier to attract empty d electrons of metals than TBC1 and RLC molecules. Generally, the higher the hardness, the greater the van der Waals force between molecular skeletons, and the molecules may entangle. Therefore, it is not easy to deform under external force [51]. That is, the intermolecular force is large, the hardness is large, and the intermolecular arrangement is closer. For contrast, the softness is opposite. By comparing the hardness (η) and softness (σ) in Table S8, it can be seen that TBC2 molecules are more difficult to deform than TBC1 and RLC molecules. The values of ΔN suggest the tendency within a set of molecules, but the absolute values are not corresponded to the reality, which means that the ΔN values are not exactly the numbers of electrons leaving the donors and entering the acceptors [52].

The dipole moment μ also helps to predict the corrosion inhibition effect of an organic molecule. The increase of the dipole moment means an increase of the deformation energy and an enhancement of the adsorption on the mild steel surface [53]. According to the theoretical parameters in Table S8, the TBCs can be tightly adsorbed on the metal surface through the chemical coordination bonds, which is consistent with the experimental results. The μ values of RLC, TBC1 and TBC2 are 8.7736 D, 16.7433 D and 25.6312 D, which are much larger than that of water molecules (1.85 D), which can replace the adsorption of water molecules on the metal surface to isolate the erosion of corrosive species.

It is noted that the protonated forms of the studied molecules are also processed molecular geometry optimization (see Fig. S15, Tables S9 and S10), since the adsorption was carried out in mixed DMSO/HCl solution. Although the electron cloudy distribution in the frontier orbitals in the protonated forms is different from that in the original neutral forms (Fig. S15(a)), the similar contrasting molecular optimization results such as the ΔN values and ΔN values are found (Table S9), which further demonstrates that the protonated studied molecules can be adsorbed to mild steel surface, and the protonated TBCs are more capable for the affinity with the metal.

It can be seen from Table S10 that the E_{HOMO} and E_{LUMO} values of protonated TBCs are generally lower than the original target molecules. It shows that after the protonation, the molecule is more stable and easier to obtain electrons from the metal surface. Fig. S15 shows that the highest and lowest occupied orbital energy levels of TBCs are mainly concentrated on the quinolone skeleton. Moreover, the protonated TBCs have lower energy gap values (ΔE, TBC1 (Protonated), 0.1120 eV, TBC2 (Protonated), 0.1040 eV), which reflects that the protonated TBCs have stronger chemical chelation with the metal substrate than the unprotonated molecules. From the electronegativity (χ), hardness (η) and softness (σ) in Table S10, it can be seen that the electronegativity of the protonated TBCs is generally stronger than that of original neutral TBCs. Thus, the electron attraction of protonated molecules to steel surface is stronger. It can also be seen that the molecular stability after the protonation is enhanced.

Furthermore, it may be a correlation between the organic molecular sizes and the ability to defend the steel surface under the destructive conditions. The larger the molecular structure size is, the greater the corrosion inhibition efficiency is [54]. Therefore, as compared with the RLC, the TBCs display the larger molecular surface areas and thus the better anticorrosion effect.

3.5. A proposed adsorption and the steel corrosion-resistance of the studied molecules

According to the reports, the anodic reaction or metal dissolution is as follows [55,56]:

$$Fe + Cl^- \rightarrow (FeCl^-)_{ads} \tag{11}$$

$$(FeCl^-)_{ads} \rightarrow (FeCl)_{ads} + e^- \tag{12}$$

$$(FeCl)_{ads} \rightarrow FeCl^+ + e^- \tag{13}$$

$$FeCl^+ + e^- \rightarrow Fe^{2+} + Cl^- \tag{14}$$

The cathodic reaction or hydrogen evolution reaction is as follows:

$$Fe + H^+ + e^- \rightarrow (FeH^+)_{ads} \tag{15}$$

$$(FeH^+)_{ads} + e^- \rightarrow (FeH)_{ads} \tag{16}$$

$$(FeH)_{ads} + H^+ + e^- \rightarrow Fe + H_2 \tag{17}$$

The adsorption mechanism of an organic molecule on the steel surface generally includes physisorption and chemisorption. First, as soon as Fe ions on mild surface are produced, the original neutral form of the RLC (some parts inside the RLC molecular skeleton can have part of negative charges due to electron cloudy density distribution) may be directly adsorbed to mild surface based on electrostatic attraction effect, van der Waals force and π-π

interactions. Besides, Cl^- ions in the adsorption medium can be pre-adsorbed to on carbon steel surface to form Cl^- anionic bridge. Thus, some protonated RLC molecules (carrying positive charge) can be further adsorbed on the pre-adsorbed Cl^- bridge formed on mild steel surface *via* the π electrons of the aromatic rings, electrostatic attraction effect and van der Waals force. Even if to the original neutral RLC molecules, they may be adsorbed on Cl^- bridge covered on steel surface (because some parts inside the RLC molecular skeleton may carry part of positive charges due to electron cloudy density distribution). These adsorption processes can be considered as the physisorption. On the other hand, the RLC carrying lone pair of electrons (N, O) of heteroatoms may chelate with the empty orbitals of iron, which thus can be adsorbed to mild steel surface to inhibit the anodic dissolution of metal working electrode. This is thought as the chemisorption. Thus, the RLC exhibits the mixed corrosion inhibition behavior on carbon steel surface in HCl solution.

For more detail description, in the presence of halide ions bridge, the adsorption and anticorrosion of the RLC can be mainly attributed to the halide ions pre-adsorbed on metal surface. Hence, the interactions between the both (RLC and Cl^-) through the electrostatic attraction, van der Waals force and π-π effect increase the adsorption coverage on the metal surface, thereby reducing the dissolution of the metal. Thus, in the first step, the RLC molecules (including the original neutral form and protonated form) are adsorbed on the metal steel surface, usually replacing one or more water molecules or chloride ions originally adsorbed on the metal surface, as shown in the Eqs. (18)–(20) [57,58]:

$$Cl^- \rightarrow (Cl^-)_{ads} \tag{18}$$

$$xInh^+ + x(Cl^-)_{ads} \rightarrow x(Cl - Inh)_{ads} \tag{19}$$

$$xInh^+ + x(H_2O)_{ads} \rightarrow x(H_2O - Inh)_{ads} \tag{20}$$

wherein $(Inh)_{ads}$ are the RLC molecules (including the original neutral and protonated forms), and x is the numbers of water molecules replaced by the inhibitor.

In a word, the steel sheet provides a positive charge in DMSO/HCl adsorption medium (because of Fe ions, resulting in pre-adsorption of chloride ions (through electrostatic attraction due to the negative charge of Cl^- ions) [59]. Therefore, the RLC (including the neutral original and protonated forms) can interact with the pre-adsorbed Cl^- ions through non-covalent interactions to produce physisorption [60].

But, the RLC (Inh) can chelate with iron ions adsorbed on the mild steel surface to form metallic iron-RLC complexes as shown in the Eq. (21) [61]:

$$Fe^{2+} + (Inh)_{ads} \rightarrow [Fe - Inh]^{2+}_{ads} \tag{21}$$

Thus, this means that the RLC can be chemically bonding *via* the unfilled orbitals of Fe atoms, and thus the chemisorption may be processed by donating the lone electron pairs of heteroatoms or by donating the π electrons (*i.e.* C—C and C—O) of the RLC and by providing the empty orbitals of Fe included in steel [62].

For contrast, such chemisorption can be more remarkable for the TBCs, because free Fe ions are reduced by the strong and rapid chemical chelation between the TBCs and Fe ions. This means that free Fe ions adsorbed on mild steel surface are largely consumed by the chemical coordination with the TBCs. Thus, the chemisorption is extremely competitive, and the physisorption on steel surface may be negligible. The metallic organic complexes of TBCs can be different hexadentate ligand compounds such as "four-to-three", "two-to-two", "two-to-one" or "one-to-one" chelation, which may be more efficiently yielded than the RLC-Fe ions complexes (Fig. S16). Thus, the proposed schematic diagram of the adsorption of the studied compounds on mild steel can be interpreted as shown in Fig. S17.

4. Conclusions

In conclusion, this study presented friendly bis/tri norfloxacin scaffold-based target branched compounds for the protection of mild steel in 1.0 $mol \cdot L^{-1}$ HCl solution based on molecular preconstruction. Meanwhile, the reference linear compound carrying a single skeleton was also synthesized. The chemical structures of the studied molecules were characterized. A number of means demonstrated that the target compounds displayed spontaneous adsorption on mild steel surface, and the compact adsorption films of the target branched molecules were formed, which could be driven by prompt and tough chemical chelation between the TBCs and Fe ions. The electrochemical analysis suggested that the TBCs exhibited superior anticorrosion of mild steel in acid medium over the RLC, which could be processed by mixed the cathodic and the anodic inhibition, while the cathodic prevention performance might be more competitive. The molecular modelling indicated that the TBCs showed the lower energy gaps of HOMO-LUMO and the larger ΔN and dipole moments than the RLC, which could account for the prominent chemisorption of the TBCs on mild steel surface, while the RLC might process a mixed physisorption and chemisorption. The molecular geometry optimization of the protonation forms of the TBCs suggests that the protonated TBCs have a stronger affinity with mild steel surface than the original netural forms. The above results presented in this study could guide us to develop large-scale norfloxacin-based compounds as green organic corrosion inhibitors for mild steel in aggressive acid environments.

Data Availability

Data will be made available on request.

Declaration of Competing Interest

The authors declare that they have no known competing financial interests or personal relationships that could have appeared to influence the work reported in this paper.

Acknowledgements

We greatly thank the National Natural Science Foundation of China (21376282, 21676035, 21878029). We also thank Chongqing Science and Technology Commission (2022NSCQ-MSX1298), H. Li thanks China Postdoctoral Science Foundation (22012T50762 & 2011M501388). Y. Shi. thanks Graduate Student Research Innovation Project, Chongqing University (CYB18046). We also thank Dr. Shenying Xu for his warm help on the molecular geometry optimization. The authors thank the warm help from Analytical and Testing Center of Chongqing University.

Supplementary Material

Supplementary material to this article can be found online at https://doi.org/10.1016/j.cjche.2023.01.015.

References

[1] O. Fiehn, W. Weckwerth, Deciphering metabolic networks, *Eur. J. Biochem.* 270 (4) (2003) 579–588.
[2] M.K. Egbo, A fundamental review on composite materials and some of their applications in biomedical engineering, *J. King Saud Univ. Eng. Sci.* 33 (8) (2021) 557–568.

[3] L.C. Zhang, L.Y. Chen, A review on biomedical titanium alloys: Recent progress and prospect, *Adv. Eng. Mater.* 21 (4) (2019) 1801215.
[4] S.J. Li, C.W. Guo, X. Wang, C. Guan, G. Chen, Corrosion inhibition coating based on the self-assembled polydopamine films and its anti-corrosion properties, *Polymers* 14 (4) (2022) 794.
[5] M.L. Zheludkevich, I.M. Salvado, M.G.S. Ferreira, Sol-gel coatings for corrosion protection of metals, *J. Mater. Chem.* 15 (48) (2005) 5099–5111.
[6] T.A. Söylev, M.G. Richardson, Corrosion inhibitors for steel in concrete: State-of-the-art report, *Constr. Build. Mater.* 22 (4) (2008) 609–622.
[7] T.M. Lv, S.H. Zhu, L. Guo, S.T. Zhang, Experimental and theoretical investigation of indole as a corrosion inhibitor for mild steel in sulfuric acid solution, *Res. Chem. Intermed.* 41 (10) (2015) 7073–7093.
[8] P. Riani, G. Garbarino, A. Infantes-Molina, E. Rodríguez-Castellón, F. Canepa, G. Busca, Hydrogen from steam reforming of ethanol over cobalt nanoparticles: Effect of boron impurities, *Appl. Catal. A Gen.* 518 (2016) 67–77.
[9] S. Shurbaji, P.T. Huong, T.M. Altahtamouni, Review on the visible light photocatalysis for the decomposition of ciprofloxacin, norfloxacin, tetracyclines, and sulfonamides antibiotics in wastewater, *Catalysts* 11 (4) (2021) 437.
[10] Y.T. Shi, L.L. Chen, S.T. Zhang, H.R. Li, F. Gao, New branched benign compounds including double antibiotic scaffolds: Synthesis, simulation and adsorption for anticorrosion effect on mild steel, *Front. Chem. Sci. Eng.* 17 (2) (2023) 167–182.
[11] K.F. Khaled, The inhibition of benzimidazole derivatives on corrosion of iron in 1 M HCl solutions, *Electrochimica Acta* 48 (17) (2003) 2493–2503.
[12] B.C. Tan, S.T. Zhang, H.Y. Liu, Y.W. Guo, Y.J. Qiang, W.P. Li, L. Guo, C.L. Xu, S.J. Chen, Corrosion inhibition of X65 steel in sulfuric acid by two food flavorants 2-isobutylthiazole and 1-(1, 3-Thiazol-2-yl) ethanone as the green environmental corrosion inhibitors: Combination of experimental and theoretical researches, *J. Colloid Interface Sci.* 538 (2019) 519–529.
[13] M. Frisch, G. Trucks, H. Schlegel, G. Scuseria, M. Robb, J. Cheeseman, G. Scalmani, V. Barone, B. Mennucci, G. Petersson, Gaussian 09, Revision D. 01, Gaussian, Inc., Wallingford CT, 2013.
[14] V.A. Adole, B.S. Jagdale, T.B. Pawar, A.B. Sawant, Experimental and theoretical exploration on single crystal, structural, and quantum chemical parameters of (*E*)-7-(arylidene)-1, 2, 6, 7-tetrahydro-8 *H*-indeno[5, 4-*b*]furan-8-one derivatives: A comparative study, *J. Chin. Chem. Soc.* 67 (10) (2020) 1763–1777.
[15] A.H. Radhi, HOMO-LUMO energies and geometrical structures effecton corrosion inhibition for organic compounds predict by DFT and PM3 methods, *NeuroQuantology* 18 (1) (2020) 37–45.
[16] C.Y. Lee, T.J. Lin, H.H. Sheu, H.B. Lee, A study on corrosion and corrosion-wear behavior of Fe-based amorphous alloy coating prepared by high velocity oxygen fuel method, *J. Mater. Res. Technol.* 15 (2021) 4880–4895.
[17] M. Tourabi, K. Nohair, M. Traisnel, C. Jama, F. Bentiss, Electrochemical and XPS studies of the corrosion inhibition of carbon steel in hydrochloric acid pickling solutions by 3, 5-bis(2-thienylmethyl)-4-amino-1, 2, 4-triazole, *Corros. Sci.* 75 (2013) 123–133.
[18] X.Z. Wang, Z. Wang, X.S. Jiang, M. Zhang, Y.F. Wang, J.G. Lv, G. He, Z.Q. Sun, *In-situ* deposition and growth of Cu_2ZnSnS_4 nanocrystals on TiO_2 nanorod arrays for enhanced photoelectrochemical performance, *J. Electrochem. Soc.* 164 (13) (2017) H863–H871.
[19] Z. Zhang, N.C. Tian, L.Z. Zhang, L. Wu, Inhibition of the corrosion of carbon steel in HCl solution by methionine and its derivatives, *Corros. Sci.* 98 (2015) 438–449.
[20] N.Z.N. Hashim, K. Kassim, Hamizah Mohd Zaki, Abdulrahman I Alharthi and Zaidi Embong, XPS and DFT investigations of corrosion inhibition of substituted benzylidene Schiff bases on mild steel in hydrochloric acid, *Appl. Surf. Sci.* 476 (2019) 861–877.
[21] D.M. Collins, T. Erinosho, F.P.E. Dunne, R.I. Todd, T. Connolley, M. Mostafavi, H. Kupfer, A.J. Wilkinson, A synchrotron X-ray diffraction study of non-proportional strain-path effects, *Acta Mater.* 124 (2017) 290–304.
[22] P. Mourya, S. Banerjee, R.B. Rastogi, M.M. Singh, Inhibition of mild steel corrosion in hydrochloric and sulfuric acid media using a thiosemicarbazone derivative, *Ind. Eng. Chem. Res.* 52 (36) (2013) 12733–12747.
[23] R.V. Siriwardane, J.A. Poston Jr, E.P. Fisher, M.S. Shen, A.L. Miltz, Decomposition of the sulfates of copper, iron (II), iron (III), nickel, and zinc: XPS, SEM, DRIFTS, XRD, and TGA study, *Appl. Surf. Sci.* 152 (3–4) (1999) 219–236.
[24] S.J. Yuan, S.O. Pehkonen, B. Liang, Y.P. Ting, K.G. Neoh, E.T. Kang, Superhydrophobic fluoropolymer-modified copper surface *via* surface graft polymerisation for corrosion protection, *Corros. Sci.* 53 (9) (2011) 2738–2747.
[25] J. Haque, V. Srivastava, M.A. Quraishi, D. Singh Chauhan, H. Lgaz, I.M. Chung, Polar group substituted imidazolium zwitterions as eco-friendly corrosion inhibitors for mild steel in acid solution, *Corros. Sci.* 172 (2020) 108665.
[26] A.H. Tantawy, K.A. Soliman, H.M. Abd El-Lateef, Novel synthesized cationic surfactants based on natural piper nigrum as sustainable-green inhibitors for steel pipeline corrosion in CO_2-3.5%NaCl: DFT, Monte Carlo simulations and experimental approaches, *J. Clean. Prod.* 250 (2020) 119510.
[27] M. Basik, M. Mobin, Chondroitin sulfate as potent green corrosion inhibitor for mild steel in 1 M HCl, *J. Mol. Struct.* 1214 (2020) 128231.
[28] A. Farhadian, A. Rahimi, N. Safaei, A. Shaabani, M. Abdouss, A. Alavi, A theoretical and experimental study of castor oil-based inhibitor for corrosion inhibition of mild steel in acidic medium at elevated temperatures, *Corros. Sci.* 175 (2020) 108871.
[29] S.K. Saha, A. Dutta, P. Ghosh, D. Sukul, P. Banerjee, Adsorption and corrosion inhibition effect of Schiff base molecules on the mild steel surface in 1 $mol{\cdot}L^{-1}$ HCl medium: A combined experimental and theoretical approach, *Phys. Chem. Chem. Phys.* 17 (8) (2015) 5679–5690.
[30] X.L. Zuo, W.P. Li, W. Luo, X. Zhang, Y.J. Qiang, J. Zhang, H. Li, B.C. Tan, Research of *Lilium brownii* leaves extract as a commendable and green inhibitor for X70 steel corrosion in hydrochloric acid, *J. Mol. Liq.* 321 (2021) 114914.
[31] M.D. Levi, D. Aurbach, Simultaneous measurements and modeling of the electrochemical impedance and the cyclic voltammetric characteristics of graphite electrodes doped with lithium, *J. Phys. Chem. B* 101 (23) (1997) 4630–4640.
[32] X.W. Zheng, S.T. Zhang, W.P. Li, L.L. Yin, J.H. He, J.F. Wu, Investigation of 1-butyl-3-methyl-1*H*-benzimidazolium iodide as inhibitor for mild steel in sulfuric acid solution, *Corros. Sci.* 80 (2014) 383–392.
[33] X.W. Zheng, S.T. Zhang, W.P. Li, M. Gong, L.L. Yin, Experimental and theoretical studies of two imidazolium-based ionic liquids as inhibitors for mild steel in sulfuric acid solution, *Corros. Sci.* 95 (2015) 168–179.
[34] I. Ahamad, S. Khan, K.R. Ansari, M.A. Quraishi, Primaquine: A pharmaceutically active compound as corrosion inhibitor for mild steel in hydrochloric acid solution, *J. Chem. Pharm. Res.* 3 (2) (2011) 703–717.
[35] F. Bentiss, M. Lebrini, M. Lagrenée, M. Traisnel, A. Elfarouk, H. Vezin, The influence of some new 2, 5-disubstituted 1, 3, 4-thiadiazoles on the corrosion behaviour of mild steel in 1 $mol{\cdot}L^{-1}$ HCl solution: AC impedance study and theoretical approach, *Electrochimica Acta* 52 (24) (2007) 6865–6872.
[36] M. Kissi, M. Bouklah, B. Hammouti, M. Benkaddour, Establishment of equivalent circuits from electrochemical impedance spectroscopy study of corrosion inhibition of steel by pyrazine in sulphuric acidic solution, *Appl. Surf. Sci.* 252 (12) (2006) 4190–4197.
[37] M. Vadi, A.O. Mansoorabad, M. Mohammadi, N. Rostami, Investigation of Langmuir, freundlich and temkin adsorption isotherm of tramadol by multi-wall carbon nanotube, *Asian J. Chem.* 25 (10) (2013) 5467–5469.
[38] V.L. Kolev, K.D. Danov, P.A. Kralchevsky, G. Broze, A. Mehreteab, Comparison of the van der waals and Frumkin adsorption isotherms for sodium dodecyl sulfate at various salt concentrations, *Langmuir* 18 (23) (2002) 9106–9109.
[39] R.J. UmplebyII, S.C. Baxter, M. Bode, J.K. BerchJr, R.N. Shah, K.D. Shimizu, Application of the Freundlich adsorption isotherm in the characterization of molecularly imprinted polymers, *Anal. Chimica Acta* 435 (1) (2001) 35–42.
[40] B. Debnath, M. Majumdar, M. Bhowmik, K.L. Bhowmik, A. Debnath, D.N. Roy, The effective adsorption of tetracycline onto zirconia nanoparticles synthesized by novel microbial green technology, *J. Environ. Manage.* 261 (2020) 110235.
[41] I.A.W. Tan, A.L. Ahmad, B.H. Hameed, Adsorption of basic dye on high-surface-area activated carbon prepared from coconut husk: Equilibrium, kinetic and thermodynamic studies, *J. Hazard. Mater.* 154 (1–3) (2008) 337–346.
[42] A. Nuhnen, C. Janiak, A practical guide to calculate the isosteric heat/enthalpy of adsorption *via* adsorption isotherms in metal-organic frameworks, MOFs, *Dalton Trans.* 49 (30) (2020) 10295–10307.
[43] H.M. Abd El-Lateef, Experimental and computational investigation on the corrosion inhibition characteristics of mild steel by some novel synthesized imines in hydrochloric acid solutions, *Corros. Sci.* 92 (2015) 104–117.
[44] F. Tezcan, G. Yerlikaya, A. Mahmood, G. Kardaş, A novel thiophene Schiff base as an efficient corrosion inhibitor for mild steel in 1.0 M HCl: Electrochemical and quantum chemical studies, *J. Mol. Liq.* 269 (2018) 398–406.
[45] M.P. Andersson, P. Uvdal, New scale factors for harmonic vibrational frequencies using the B3LYP density functional method with the triple-zeta basis set 6–311+G(d, p), *J. Phys. Chem. A* 109 (12) (2005) 2937–2941.
[46] S.K. Saha, M. Murmu, N.C. Murmu, P. Banerjee, Evaluating electronic structure of quinazolinone and pyrimidinone molecules for its corrosion inhibition effectiveness on target specific mild steel in the acidic medium: A combined DFT and MD simulation study, *J. Mol. Liq.* 224 (2016) 629–638.
[47] L. Guo, Z.S. Safi, S. Kaya, W. Shi, B. Tüzün, N. Altunay, C. Kaya, Anticorrosive effects of some thiophene derivatives against the corrosion of iron: A computational study, *Front. Chem.* 6 (2018) 155.
[48] A. Zarrouk, B. Hammouti, A. Dafali, M. Bouachrine, H. Zarrok, S. Boukhris, S.S. Al-Deyab, A theoretical study on the inhibition efficiencies of some quinoxalines as corrosion inhibitors of copper in nitric acid, *J. Saudi Chem. Soc.* 18 (5) (2014) 450–455.
[49] R.G. Pearson, Absolute electronegativity and hardness: Application to inorganic chemistry, *Inorg. Chem.* 27 (4) (1988) 734–740.
[50] R.F. Peterson, D.F. Treagust, P. Garnett, Development and application of a diagnostic instrument to evaluate grade-11 and-12 students' concepts of covalent bonding and structure following a course of instruction, *J. Res. Sci. Teach.* 26 (4) (1989) 301–314.
[51] F.J. Baltá Calleja, Microhardness relating to crystalline polymers. Characterization of Polymers in the Solid State I: Part A: NMR and Other Spectroscopic Methods Part B: Mechanical Methods, Springer Berlin Heidelberg, Berlin, Heidelberg, 1985, pp. 117–148.
[52] F. Meyers, S.R. Marder, B.M. Pierce, J.L. Bredas, Electric field modulated nonlinear optical properties of donor-acceptor polyenes: Sum-over-states investigation of the relationship between molecular polarizabilities (alpha., beta., and. gamma.) and bond length alternation, *J. Am. Chem. Soc.* 116 (23) (1994) 10703–10714.
[53] T. Arslan, F. Kandemirli, E.E. Ebenso, I. Love, H. Alemu, Quantum chemical studies on the corrosion inhibition of some sulphonamides on mild steel in acidic medium, *Corros. Sci.* 51 (1) (2009) 35–47.
[54] F.A. Azeez, O.A. Al-Rashed, A. Abdel Nazeer, Controlling of mild-steel corrosion in acidic solution using environmentally friendly ionic liquid inhibitors: Effect of alkyl chain, *J. Mol. Liq.* 265 (2018) 654–663.
[55] A.H. Mostafatabar, G. Bahlakeh, B. Ramezanzadeh, A. Dehghani, M. Ramezanzadeh, A comprehensive electronic-scale DFT modeling, atomic-

level MC/MD simulation, and electrochemical/surface exploration of active nature-inspired phytochemicals based on *Heracleum persicum* seeds phytoextract for effective retardation of the acidic-induced corrosion of mild steel, *J. Mol. Liq.* 331 (2021) 115764.
[56] A.P.S. Kaban, A. Ridhova, G. Priyotomo, B. Elya, A. Maksum, Y. Sadeli, S. Sutopo, T. Aditiyawarman, R. Riastuti, J.W. Soedarsono, Development of white tea extract as green corrosion inhibitor in mild steel under 1 M hydrochloric acid solution, *East. Eur. J. Enterp. Technol.* 2 (6 (110)) (2021) 6–20.
[57] J.M. Bastidas, J.L. Polo, E. Cano, C.L. Torres, Tributylamine as corrosion inhibitor for mild steel in hydrochloric acid, *J. Mater. Sci.* 35 (11) (2000) 2637–2642.
[58] M. Jokar, T.S. Farahani, B. Ramezanzadeh, Electrochemical and surface characterizations of morus alba pendula leaves extract (MAPLE) as a green corrosion inhibitor for steel in 1 M HCl, *J. Taiwan Inst. Chem. Eng.* 63 (2016) 436–452.
[59] M. Rbaa, F. Benhiba, A.S. Abousalem, M. Galai, Z. Rouifi, H. Oudda, B. Lakhrissi, I. Warad, A. Zarrouk, Sample synthesis, characterization, experimental and theoretical study of the inhibitory power of new 8-hydroxyquinoline derivatives for mild steel in 1.0 M HCl, *J. Mol. Struct.* 1213 (2020) 128155.
[60] E. Altunbaş Şahin, R. Solmaz, İ.H. Gecibesler, G. Kardaş, Adsorption ability, stability and corrosion inhibition mechanism of phoenix dactylifera extrat on mild steel, *Mater. Res. Express* 7 (1) (2020) 016585.
[61] E.E. Oguzie, Y. Li, F.H. Wang, Corrosion inhibition and adsorption behavior of methionine on mild steel in sulfuric acid and synergistic effect of iodide ion, *J. Colloid Interface Sci.* 310 (1) (2007) 90–98.
[62] J. Aslam, R. Aslam, I.H. Lone, N.R.E. Radwan, M. Mobin, A. Aslam, M. Parveen, A. A. Al-Freedi, A.A. Alzulaibani, Inhibitory effect of 2-nitroacridone on corrosion of low carbon steel in 1 $mol \cdot L^{-1}$ HCl solution: An experimental and theoretical approach, *J. Mater. Res. Technol.* 9 (3) (2020) 4061–4075.